CHAPTER

14

Mathematical Modeling and Analysis of Intracellular Signaling Pathways

Paul D. Smolen, Douglas A. Baxter, and John H. Byrne

As discussed in Chapter 12, sequences of biochemical reactions termed intracellular signaling pathways transmit signals from the extracellular medium to cytoplasmic or nuclear targets. Ca^{2+} influx is one such signal. Binding of hormones, neurotransmitters, or growth factors to receptors is also a signal. Intracellular signaling pathways translate these signals into effects on the rates of specific cellular processes, such as the transcription of particular genes. In this way, extracellular signals can modulate long-term processes, such as neuronal growth and the formation of long-term memory. It is possible that, in addition to electrical activity, biochemical signals between neurons may be usefully regarded as a conduit of information within the nervous system (Katz and Clemens, 2001). This chapter provides an overview of concepts and techniques necessary to describe and analyze the operation of intracellular signaling pathways with concise mathematical language. By use of these techniques, it is possible to model series (either unbranched or branched) of enzyme reactions. Since such series are commonly termed *metabolic pathways* or *biochemical pathways*, we often use these terms as well as *signaling pathways*.

Because of recent technological advances, information on the operation of intracellular signaling pathways and relationships to long-term neuronal changes is rapidly accumulating. For example, the expression of large groups of genes subsequent to activation of signaling pathways by hormones, neurotransmitters, or drugs can be followed with microarrays ("DNA chips") of specific DNA sequences. Mathematical modeling can provide a conceptual framework to assemble these complex data into concise pictures of the structure and operation of signaling or metabolic pathways. Although all biologists work with "word models" that describe for them how a system works, intuition fails to adequately deal with complex biochemical systems, and equations are needed to make "word models" rigorous and check them for consistency (Marder, 2000). Furthermore, once model equations are developed, computer simulations or algebraic calculations can display and predict the behavior of complex biochemical systems more accurately and completely than can intuition. This is particularly true if the individual biochemical reactions are ***nonlinear***. A reaction is termed linear if its rate is directly proportional to the concentrations of reactants or of other components such as allosteric effectors of an enzyme. If the reaction rate varies in a more complex manner, the reaction is nonlinear. Computer simulations of equations describing nonlinear reactions commonly display unexpected and complex behaviors (see also Chapter 7, Box 7.4).

Models also help in understanding the effects of multiple feedback interactions within intracellular signaling pathways. Such interactions might include alteration of enzyme activities due to allosteric binding of reaction products further along in a pathway. Time delays, such as are required for macromolecular synthesis and intracellular transport, also add complexity to the behavior of biochemical systems. For example, time delays can be critical for sustaining oscillations in reaction rates and in metabolite concentrations. Such effects of time delays are often nonintuitive and can be appreciated only with a mathematical model.

A model is particularly valuable if it succeeds in reproducing, or predicting, behaviors in addition to those it was originally constructed to replicate (Mark, 2000). For example, the Hodgkin–Huxley model of voltage-gated currents was constructed to reproduce

the properties of those currents as observed in experiments with each current isolated (Hodgkin and Huxley, 1952). That the model would, in addition, succeed in simulating an action potential was not evident a priori, and was of great significance. The simulation helped to confirm that the action potential resulted from the voltage and time dependence of the known voltage-gated currents in the squid axon. The success of this model also helped to establish the utility of mathematical descriptions of neuronal properties. Chapters 5 and 7 discuss the Hodgkin–Huxley model in more detail.

Models are also valuable in establishing principles governing the behavior of biochemical systems. Modeling of signaling pathways and gene regulation has established a unifying principle that ***feedback interactions*** commonly underlie complex behaviors. Negative feedback, in which a biochemical species acts to inhibit its own production, often underlies oscillations in biochemical concentrations or gene expression rates. This principle will be illustrated by examples throughout the chapter.

Biochemical models can be constructed at several levels of detail. The most detailed is the ***stochastic*** level. Here, one keeps track of the numbers of each type of molecule over time. Such models can be very important if the average numbers of key macromolecules are low. For example, only tens or hundreds of molecules of specific transcription factors or mRNAs may be present. Then, random variations in molecule numbers due to the creation or destruction of individual molecules can have considerable consequences. For example, irreducible individual variability in laboratory animals may be due to random fluctuations in the numbers of key transcription factors and mRNAs during embryonic development (Gartner, 1990).

Lack of experimental data for molecule numbers and for their fluctuations, however, limits the applicability of stochastic models. More commonly, the approximation is made that biochemical concentrations can be written as continuous variables, not as discrete numbers of molecules. The ***continuous*** level of modeling uses differential equations for the rates of change of these biochemical concentration variables. At this level, familiar quantities from biochemical kinetics—rate constants, Michaelis constants, enzyme activities—govern the changes in concentrations. Most models discussed in this chapter use this continuous approximation. Computer simulations numerically integrate the differential equations to follow concentrations over time, and the simulations are compared with experimental data. Values of model parameters, such as binding constants and rate constants, are adjusted to improve agreement between simulation and experiment. Finally, if the experimental data are incomplete, a ***logical*** or ***boolean*** approach may be used. Here, genes or enzymes are simply regarded as switches that are either ON or OFF. For example, this approach has been used to model the changing activities of large numbers of genes during development or cell differentiation.

The choice of which level of modeling to use is determined mainly by the hypothesis to be tested. For example, if a specific enzyme is believed to be rate-limiting for the progress of a biochemical pathway, it is appropriate to use the continuous level of modeling. The activity of the enzyme will be a parameter determining the rate of the reaction. Then it is possible to explore, in a computer simulation, how changing the activity affects the concentrations both of the reaction product and of all chemical species "downstream" in the pathway.

Usually, it is desirable to construct the simplest model capable of capturing the features of the system most relevant to the hypothesis being tested. Such a model highlights the essential features without adding irrelevant details. For example, fluctuations in molecule numbers may not be important when average molecule numbers are large. A method based on separation of rapid and slow biochemical reactions is also often used to simplify models. It is often useful to reduce the number of equations by assuming that the fastest biochemical reactions in a pathway are always near equilibrium.

Another important distinction is between ***quantitative models***, which describe the structure and behavior of specific intracellular biochemical pathways, and **qualitative models**, which generally have fewer equations and are constructed to embody biochemical elements common to many pathways of reactions. Such elements include feedback interactions, random fluctuations in molecule numbers, and formation of multiprotein complexes containing enzymes or transcription factors. This chapter relies primarily on qualitative models. Such models illustrate how typical biochemical elements can give rise to specific types of pathway dynamics, that is, pathway behavior over time. These behaviors include oscillations in reaction rates, or switching between steady states of reaction rates and macromolecule concentrations. As one example, qualitative models of glycolysis incorporate feedback activation of the key glycolytic enzyme phosphofructokinase by its reaction product ADP (Goldbeter, 1996). These models have established that the feedback is important for sustaining oscillations in the rate of glycolysis (Dano *et al.*, 199

The discussion of methods for modeling intracellular signaling pathways begins with a basic process common to all pathways: the transport of signaling molecules within the cell. The mechanism of transport can strongly affect the behavior of signaling pathways. Following the discussion of transport, techniques for modeling sequences of biochemical reactions are discussed and illustrated with examples relevant to neuronal function. The unifying principle that feedback interactions commonly underlie complex behaviors of biochemical systems is developed in the succeeding section. Models for multiple activity states of Ca^{2+}/calmodulin-activated protein kinase II and for oscillations in the rate of glycolysis are discussed. Also, models can help assess the importance of interactions between signaling pathways. A metabolite from one pathway may be a substrate for a reaction in another pathway. Some examples are presented.

At this point, two general issues that need to be considered whenever a biochemical system is modeled are discussed. First, techniques for estimating model parameter values from data are discussed, and the limitations of these techniques for determining *in vivo* values are assessed. Also, the importance and methodology of assessing the sensitivity of model behavior to parameter values are discussed. Second, the method for simplifying models based on separation of rapid and slow biochemical reactions is discussed, and illustrated by deriving the standard Michaelis–Menten equation for the rate of product formation by an irreversible enzyme.

Following these general topics, specific topics important for many, but not all, models of biochemical pathways are addressed. A method for determining which parameters are key control points for the flux of metabolite through a pathway is discussed. Also, rapid ***stochastic fluctuations*** in the numbers of important molecules can significantly affect enzymes or genes regulated by those molecules. A method for modeling these fluctuations is discussed. Finally, methods for modeling the regulation of gene expression are discussed. Models of transcriptional regulation are of particular importance since regulation of gene expression is an essential part of signaling pathways that mediate long-term changes in cell properties. An example is long-term strengthening of synapses, which requires transcription and appears to be essential for the formation of long-term memory (Martin *et al.*, 2000). (see also Chapter 18).

For further study, a selection of textbooks are listed at the beginning of the reference list. These provide a more comprehensive treatment of the ways in which models can be constructed and analyzed, and of the mathematics required, including differential equations.

METHODS FOR MODELING INTRACELLULAR SIGNALING PATHWAYS

Intracellular Transport of Signaling Molecules Can Be Modeled at Several Levels of Detail

Intracellular messages can be transmitted by ions such as Ca^{2+}, by small molecules such as cAMP, or by movement of macromolecules such as enzymes and transcription factors. Modeling intracellular transport of these species is of great importance for understanding the operation of intracellular signaling pathways.

Passive Diffusion Dominates for Ions and Small Molecules

Intracellular transport of ions and small molecules is generally diffusive. Therefore, modeling of ***diffusive transport***—due to movement caused by random thermal collisions with other molecules—is discussed in some detail. Passive diffusion of macromolecules can be modeled by the same equations as for small molecules, but with much smaller diffusion coefficients. More detailed "electrodiffusion" models are used to consider movement of charged molecules due to electric potential gradients within neurons.

The discussion focuses on techniques for modeling the diffusion of a specific ion, Ca^{2+}. The intracellular movement of Ca^{2+} has been extensively studied experimentally and modeled in a variety of ways. The same equations and the same techniques for numerical simulations can be applied to diffusion of other small molecules and ions. The diffusion coefficient must be corrected for differences in molecular weight. For free diffusion in aqueous solution, the diffusion coefficient is inversely proportional to the cube root of molecular weight. However, diffusion *in vivo* is not free, because ***buffering***, or binding of small molecules or ions to sites on macromolecules, is common throughout the cytoplasm. Buffering generally decreases diffusion coefficients below values in aqueous solution.

Concise Models of Ca^{2+} Exchange between Compartments Represent Ca^{2+} Release and Uptake Mechanisms

As discussed in Chapter 12, both free Ca^{2+} and Ca^{2+} bound to proteins such as calmodulin can activate numerous enzymes within intracellular signaling pathways. Therefore, many investigators have

modeled aspects of the movement of Ca^{2+} from the plasma membrane to other regions. Two basic approaches are used. The simplest considers only Ca^{2+} exchange across membranes that separate intracellular compartments. The exchange can be driven by passive diffusion or by ion "pump" proteins that use ATP. Distinct membrane-bound compartments are each assigned a **pool** of Ca^{2+}. For example, cytoplasmic Ca^{2+}, Ca^{2+} in the endoplasmic reticulum, mitochondrial Ca^{2+}, and Ca^{2+} in the nucleus might each be considered to form a distinct "pool." Cytoplasmic Ca^{2+} could communicate with all the other pools. The time course of the amounts of Ca^{2+} in each pool is followed during computer simulations. In the second, more computationally intensive approach, the spaces within intracellular compartments are modeled as small volume elements, and the Ca^{2+} concentration in each element is followed separately. Diffusion of Ca^{2+} within compartments or across membranes that separate compartments can be modeled as fluxes between volume elements. This approach is required if it is necessary to model concentration gradients within the cytoplasm or other compartments.

Suppose a single pool describes cytoplasmic Ca^{2+}. A single ***ordinary differential equation*** is then written to describe the rate of change of cytoplasmic Ca^{2+} concentration, $[Ca^{2+}_{cyt}]$. The rate of change is assumed proportional to Ca^{2+} influx across the plasma membrane. It also depends on rates of exchange between cytoplasmic Ca^{2+} and Ca^{2+} in intracellular compartments such as the endoplasmic reticulum:

$$\frac{d[Ca^{2+}_{cyt}]}{dt} = \lambda I_{Ca} + k_{exch}\left([Ca^{2+}_{ER}] \pm [Ca^{2+}_{cyt}]\right) \pm k_{Ca}[Ca^{2+}_{cyt}]. \quad (1)$$

In Eq. 1, the first term on the right-hand side describes Ca^{2+} influx across the plasma membrane through an ion channel or set of channels. A scaling constant, here denoted by λ, is required to convert Ca^{2+} current to a rate of change of Ca^{2+} concentration. As discussed in Chapter 7, detailed expressions can be used to describe the voltage and time dependence of such ionic currents. The second term on the right-hand side of Eq. 1 describes exchange of Ca^{2+} between the endoplasmic reticulum (ER) and the cytoplasm. For illustrative purposes this term is very simple: it is merely proportional to the concentration difference between the two Ca^{2+} pools.

In models of specific cell types more detailed kinetic expressions might be needed to describe Ca^{2+} release from the ER. For example, special expressions are necessary to describe stimulation of ER Ca^{2+} release by the second messenger molecule inositol 1, 4, 5-triphosphate (IP_3). Recent models (Wagner *et al.*, 1998; Li and Rinzel, 1994). describe Ca^{2+} release through the IP_3 receptor on the ER as increasing steeply with the third or fourth power of the cytoplasmic IP_3 concentration. Ca^{2+} release through the IP_3 receptor also increases steeply with the cytoplasmic Ca^{2+} concentration. This is ***positive feedback***, because an initial increase in cytoplasmic Ca^{2+} stimulates further release of Ca^{2+} from the ER and a further increase in cytoplasmic Ca^{2+}. Such positive feedback can help to generate Ca^{2+} waves and oscillations in a variety of cell types (Wagner *et al.*, 1998; Li and Rinzel, 1994; Nakamira *et al.*, 1999).

The last term in Eq. 1 describes Ca^{2+} extrusion across the membrane as a simple first-order process. However, a more detailed expression may be preferred if data concerning rates of extrusion are available to give estimates for the parameters in such an expression. For example, the expression

$$\pm k_{Ca}\frac{[Ca^{2+}_{cyt}]}{[Ca^{2+}_{cyt}] + K} \quad (2)$$

describes Ca^{2+} extrusion across the plasma membrane by a saturable ion pump. In Eq. 2, the parameter K gives the value of $[Ca^{2+}]$ at which the pump rate is half-maximal. Saturable pumps driven by ATP hydrolysis are present in many cell types. A more complicated expression,

$$-k_{Ca}([Ca^{2+}_{cyt}]^2[Na^{+}_{external}]^3 - [Ca^{2+}_{external}]^2[Na^{+}_{cyt}]^3), \quad (3)$$

is sometimes used to describe removal of Ca^{2+} by a $Na^+ - Ca^{2+}$ exchanger present in neurons and other excitable cells (De Schutter and Smolen, 1998). This exchanger brings Na^+ into the cytoplasm while concurrently removing Ca^{2+}. In Eq. 3 there are two terms. The first term describes Ca^{2+} removal and the second term is necessary because the exchanger can also operate in reverse, bringing in Ca^{2+}. The powers of Na^+ and Ca^{2+} concentrations reflect the mechanism of the exchanger protein, which undergoes repeated cycles of conformational change, bringing in approximately three Na^+ ions per cycle while extruding two Ca^{2+} ions.

To simulate changes in Ca^{2+} concentration as described by a differential equation such as Eq. 1, ***Euler's method*** is often used. A reasonable initial value for $[Ca^{2+}_{cyt}]$ is chosen (such as 50 nM, which is in the range expected if a neuron is hyperpolarized and there is little Ca^{2+} influx through ion channels). Then, at each small step in time, one calculates the rate of change of $[Ca^{2+}_{cyt}]$ in terms of the quantities on the right-hand side of Eq. 1. The rate of change is mul-

tiplied by the size of the time step and the result is added to $[Ca^{2+}_{cyt}]$. This procedure is repeated until a time length sufficient to display the behavior of $[Ca^{2+}_{cyt}]$ during neuronal activity has been simulated. To determine whether the time step chosen is small enough, the entire simulation is typically repeated with a time step approximately one-third as long, and if the behavior of $[Ca^{2+}_{cyt}]$ does not vary significantly, the larger time step is considered adequate. This simple method of numerical integration can be applied to any differential equation discussed in this chapter. More complex integration methods also exist and these may, for many models, allow faster simulations. Textbooks on numerical analysis (Burden and Faires, 1993) can be consulted for details about these methods.

To Model Diffusion in Realistic Detail, Standard but Complex Equations Can be Used

To more accurately model the intracellular diffusion of Ca^{2+}, other ions, or small molecules, the intracellular space must be ***discretized***, or divided into small volume elements. The evolution of the Ca^{2+} concentration within each element must be simulated. Such discretization is the standard method for simulating the partial differential equation that describes diffusion within an extended region. A common implementation uses cubic or rectangular volume elements. The cytoplasm or other region of interest is approximated by a large set of small boxes in x, y, z space. The overall set is chosen to have a shape that is a reasonable representation of the region of interest. For example, an approximate sphere with a "boxy" boundary may be used to represent the nucleus. The flux of Ca^{2+} between two cubic boxes depends on the cube size and the Ca^{2+} diffusion coefficient, D_{Ca}. The dependence is

$$Flux_{1\to 2} = D_{Ca}\frac{A}{L}\left([Ca^{2+}]_1 \pm [Ca^{2+}]_2\right). \qquad (4)$$

In Eq. 4, L is the length of a cube edge, and A ($= L^2$) is the area of a cube face. $[Ca^{2+}]_1$ refers to the Ca^{2+} concentration in cube 1. A variant of Eq. 4 is used for rectangular boxes. Although Eq. 4 as written describes the diffusion of only free Ca^{2+}, the same type of equation can be used to describe the diffusion of Ca^{2+} bound to calmodulin or other species. Simulations using Eq. 4 can use Euler's numerical integration method, as for Eq. 1. At each small time step, the flux of Ca^{2+} given by Eq. 4 is multiplied by the size of the time step, and the resulting quantity is added to the preceding Ca^{2+} concentration in volume element 2 while also being subtracted from the preceding Ca^{2+} concentration in volume element 1. At each time step this calculation must be repeated for every pair of adjacent volume elements in the system.

In one application (Simon and Llinas, 1985), Eq. 4 was used to simulate dynamics of localized Ca^{2+} peaks near clusters of open Ca^{2+} channels. It was found that near the cytoplasmic mouth of a channel, free Ca^{2+} concentrations could reach values of tens of micromolar, or higher. These ***Ca^{2+}*** microdomains form and dissipate within microseconds of channel openings/closings. Enzymes or other proteins positioned near clusters of channels can serve as sensors for such elevations of concentration, and intracellular signaling pathways could thereby be activated. For example, pathway activation could lead to local synaptic potentiation or depression. The importance of Ca^{2+} microdomains for the release of neurotransmitter was discussed in Chapter 8.

Modeling diffusion with rectangular volume elements has the disadvantage of requiring very large amounts of computer time and memory because of the large number of elements required to discretize space in three dimensions. For example, if each axis is to be divided into 100 parts, a total of 1,000,000 volume elements are needed. A great reduction in time and memory requirements can be achieved if the biological system can be approximated by a model where, because of an inherent ***symmetry***, diffusion in one or two dimensions can be neglected. Then only two or one dimensions, respectively, need to be divided into small volume elements.

For example, suppose diffusion within a spherically symmetric compartment, such as an ideal soma, is being modeled. If Ca^{2+} is assumed to enter and leave at equal rates over all regions of the outer surface, then Ca^{2+} concentration is independent of both angle coordinates within the sphere. Then, only the radial dimension needs to be discretized because diffusion is only along the radial direction from the surface to the center. The compartment can be divided radially into thin, concentric spherical shells (Fig. 14.1A). The concentration changes in each shell due to fluxes of Ca^{2+} between shells are simulated. An equation analogous to Eq. 4 is used, and Euler's integration method can be used. Computer algorithms for these simulations have been published. The algorithm in Blumenfeld *et al.* (1992) is particularly straightforward to implement.

As a second example in which symmetry reduces the number of dimensions that need to be discretized, consider a portion of a neuronal dendrite or axon, which can be modeled as a cylindrical compartment. Suppose Ca^{2+} is assumed to enter one end and leave at the other end, without significant influx from the

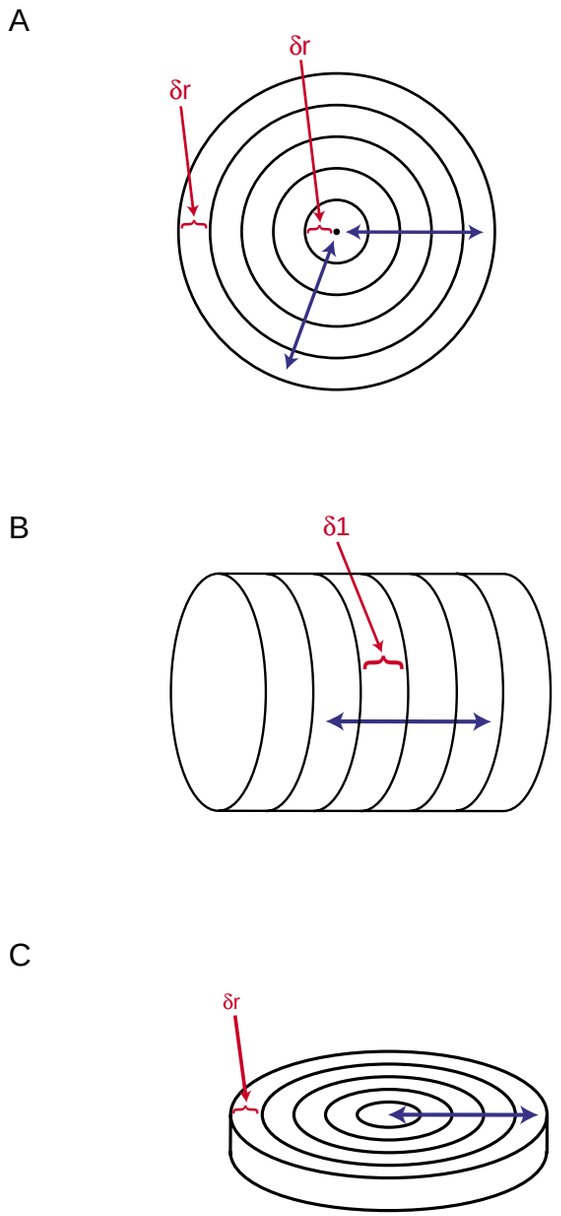

FIGURE 14.1 Symmetry can allow advantageous division of spatial regions into volume elements to model diffusion. (A) Spherically symmetric diffusion. A spherical region is divided into thin concentric cells of width δr. Diffusion of molecules between shells occurs in the radial direction (blue arrows). (B) Longitudinal diffusion in a cylinder (blue arrow). The cylinder is divided into thin slabs of width δl. (C) Radially symmetric diffusion in a disk-shaped region that approximates a synaptic cleft. The disk is divided into concentric annuli of width δr.

sides. Then Ca^{2+} gradients across the width of the cylinder can be neglected, and Ca^{2+} diffusion occurs only along the length of the cylinder. Thus, only the dimension of length needs to be divided into volume elements. The cylinder can be divided into thin slabs, and the evolution of the concentration in each slab simulated (Fig. 14.1B). Also, consider a different cylindrical compartment for which Ca^{2+} flux through the side face, but not through the ends, is significant. If all regions of the face are assumed homogenous, then concentration gradients will develop only in the radial direction, from the outer surface to the center. Thus, the cylinder may be divided into a series of thin, concentric cylindrical shells. The algorithm in Blumenfeld *et al.* (1992) can readily be adapted to this case. As a last example of a useful symmetry, diffusion of neurotransmitter within a synaptic cleft has been modeled by describing the cleft as a thin disk-shaped region and neglecting the gradient of neurotransmitter across the cleft. If neurotransmitter is released at the center, only diffusion in the radial direction needs to be considered. The disk can be discretized into concentric annular rings (Fig. 14.1C) and diffusion between the rings is simulated. However, if neurotransmitter is released anywhere besides the center of the disk, diffusion in the angular direction cannot be neglected, and simulation requires discretization in both the radial and the angular dimensions.

These methods for modeling diffusion all assume that ionic movement is driven by concentration gradients to a much greater extent than by electrical potential gradients. This may not hold true within small structures such as dendritic spines. For example, influx of ions during electrical activity might cause large potential differences between the spine head and the dendritic shaft. The ***electrodiffusion*** modeling approach is more accurate for such situations. This approach uses more general and complex equations, with terms to account for ion movement due to diffusion and due to potential-driven drift. As an example, the Nernst–Planck equation and discretization into small volume elements have been used to model diffusion of several ionic species within a spine and the adjacent dendrite (Qian and Sejnowski, 1990). When constructing electrodiffusion models, it is necessary to carefully consider which charged ions or molecules are likely to play the largest roles in carrying charges and dynamically altering potential gradients. Both the concentrations and mobilities of common charged species need to be considered when making these assessments.

Buffering Must Be Considered in Models

Binding of ions or small molecules to macromolecules can greatly slow diffusion. For example, a Ca^{2+} ion spends much of its time bound, so that the diffusion of Ca^{2+} ions is much slower in the cell than in water. Other ions, and small molecules, tend to have fewer binding sites than does Ca^{2+}, so that their diffusion is not slowed to such an extent. For example,

there are relatively few intracellular binding sites for the second messenger IP_3. Therefore, diffusion of IP_3 can be considerably more rapid than diffusion of Ca^{2+}, even though the molecular weight of a Ca^{2+} ion is much lower (Jaffrq and Keizer, 1995).

For a given class of Ca^{2+} binding sites, denoted S, and present at a total concentration S_{tot}, consider equilibration between free and bound Ca^{2+}. By use of standard chemical kinetic notation, the dissociation and association rate constants for formation of S–Ca^{2+} complex are respectively denoted k_b and k_f. Equilibration is then described by the differential equation

$$\frac{d[Ca^{2+}]_{free}}{dt} = k_b[S \pm Ca^{2+}] \pm k_f\left(S_{tot} \pm [S \pm Ca^{2+}]\right) [Ca^{2+}]_{free} \quad (5)$$

In Eq. 5, [S–Ca^{2+}] denotes the concentration of S–Ca^{2+} complex, $[Ca^{2+}]_{free}$ denotes the concentration of unbound Ca^{2+}, and the expression S_{tot} – [S–Ca^{2+}] gives the concentration of free S sites. An equilibrium dissociation constant, K, is defined as k_b / k_f. When $[Ca^{2+}]_{free}$ is at equilibrium and equal to K, half of the sites S are occupied by Ca^{2+}. This can be seen as follows. At equilibrium, the system is unchanging, so that

$$\frac{d[Ca^{2+}]_{free}}{dt} = 0.$$

Therefore, at equilibrium, the right-hand side of Eq. 5 can be set equal to zero. Then a rearrangement gives

$$K = k_b / k_f = \frac{[S][Ca^{2+}]_{free}}{[S \pm Ca^{2+}]}. \quad (6)$$

If $[Ca^{2+}]_{free} = K$, Eq. 6 simplifies to

$$\frac{[S]}{[S \pm Ca^{2+}]} = 1;$$

i.e., 50% of the sites are occupied by Ca^{2+}.

If binding and unbinding of Ca^{2+} are fast processes (large k_f and k_b), then a ***rapid equilibrium*** approximation is justified. This assumes that the difference between the two terms on the right-hand side of Eq. 5 is always small in comparison with the absolute magnitudes of either term. Thus the terms can be considered equal for practical purposes. The right-hand side of Eq. 5 is therefore again set equal to zero. The equilibrium constant K is k_b/k_f. There are two conservation conditions that express the total concentration of buffer sites S_{tot} and the total Ca^{2+} concentration C_{tot} in terms of the individual biochemical species:

$$S_{tot} = [S] + [S \pm Ca^{2+}]$$

and

$$C_{tot} = [Ca^{2+}]_{free} + [S–Ca^{2+}].$$

Under these conditions, the concentration of free S can be expressed as

$$[S] = [Ca^{2+}]_{free} + S_{tot} - C_{tot}. \quad (7)$$

Using Eq. 6 for the equilibrium constant K, and using Eq. 7, an equation can be written that expresses $[Ca^{2+}]_{free}$ in terms of constant parameters and the total calcium concentration:

$$\frac{[S][Ca^{2+}]_{free}}{[S \pm Ca^{2+}]} = \frac{\left([Ca^{2+}]_{free} + S_{tot} \pm C_{tot}\right)[Ca^{2+}]_{free}}{C_{tot} \pm [Ca^{2+}]_{free}} = K. \quad (8)$$

From Eq. 8, it is possible to solve for $[Ca^{2+}]_{free}$ in terms of the other quantities.

Euler's integration method, discussed above, can be used for simulations of the evolution of the concentrations of free and bound Ca^{2+}. At each time step of the simulation, the total Ca^{2+} concentration C_{tot} can first be updated by considering processes of Ca^{2+} influx into or removal from the cytoplasm. To generate a time course of free Ca^{2+}, Eq. 8 can then be used to update $[Ca^{2+}]_{free}$. Why use this somewhat cumbersome equation? Because if binding of Ca^{2+} to S is much faster than influx or removal of Ca^{2+} from the cytoplasm, then assuming binding to be always at equilibrium (Eq. 8) can allow much larger time steps to be taken in simulations, saving much computer time. The time steps only need to be small relative to Ca^{2+} influx or removal rates. Equation 8 is an example of a more general principle. Assuming that rapid biochemical processes are always at equilibrium can greatly simplify a model by reducing the number of differential equations.

When multiple classes of buffer sites (S_1, S_2, . . .) are present, each class will have its own values of the parameters k_f, k_b, and S_{tot}. An analog of Eq. 5 can be written. The right-hand side of the analog contains separate terms for each value of k_f and k_b for each class. However, the rapid-equilibrium approximation is no longer useful in simulations, because with multiple buffers, Eq. 8 becomes too complex to allow for savings in computer time.

Experimental data suggest that, to a reasonable approximation, total intracellular Ca^{2+} buffering can often be thought of as due to one or two "lumped" buffering species, or classes of buffer sites (Zhou and Neher, 1993). The effect of each species is described by

different values of the equilibrium constant K and the total site concentration S_{tot}. A useful experimental quantity that helps determine values of K and S_{tot} is the ***buffering capacity***. This is the ratio of the change in total (free + bound) Ca^{2+} to the change in free Ca^{2+} when a small amount of Ca^{2+} is added to the cytoplasm. In an analysis of Ca^{2+} buffering in adrenal chromaffin cells (Zhou and Neher, 1993). it was found that buffering could be described by two "lumped" species: one immobile with a buffering capacity of ~30, and the other slowly diffusing and having a buffering capacity of ~10. In neurons, similar or greater values apply. Detailed calculations using these estimates of buffering capacity suggest that ~98–99% of cytosolic Ca^{2+} is bound in chromaffin cells (Zhou and Neher, 1993) and presumably in neurons.

Molecular probes have been developed that monitor the intracellular movement of Ca^{2+} and other ions or small molecules, including Mg^{2+}, Zn^{2+}, and cAMP. For example, dyes such as Fura-2 have a fluorescence emission spectrum that is altered by Ca^{2+} binding. Experimental data characterizing Ca^{2+} gradients and movement are obtained by monitoring changes in the fluorescence of such dyes. Data obtained with such probes are vital to refining mathematical models that include transport. Models to simulate such data need to consider the diffusion of all important species including dye with and without bound Ca^{2+}. Buffering due to introduced probes can have complex effects on the diffusion coefficients of ions and small molecules (Wagner and Keizer, 1994). Introduction of a small probe molecule that binds Ca^{2+} can speed up the net rate of Ca^{2+} diffusion, even though the free concentration of Ca^{2+} is decreased. This occurs because, after the probe is added, a significant fraction of total Ca^{2+} is bound to highly mobile probe molecules instead of poorly mobile macromolecules.

Models that incorporate the dynamics of IP_3—induced Ca^{2+} release, Fura–2 diffusion, and Ca^{2+} buffering—have simulated experimental characterizations of intracellular Ca^{2+} waves following hormonal or electrical stimulation. These models—or any model—are most useful if they can predict the results of future experiments. If the predictions bear out, the model gains credibility as a valid physiological description. For example, one recent investigation (Fink *et al.*, 2000) quantitatively predicted alterations in Ca^{2+} waves due to microinjection of excess buffer or photorelease of intracellular IP_3.

Details of buffer and Ca^{2+} diffusion can be disregarded if Ca^{2+} dynamics are being modeled using separate intracellular "pools" (Eq. 1) with Ca^{2+} exchange across membranes separating pools. In this situation, it is common to regard the ratio of free Ca^{2+} to total Ca^{2+} as fixed within each pool. For example, if the overall buffering capacity of the cytoplasm is in the range of 100, a fixed ratio of 0.01 would be appropriate. In this case, only 1/100th of the Ca^{2+} entering or leaving the pool is reflected as a change in the concentration of free Ca^{2+}. The modification of Eq. 1 required is

$$\frac{d[Ca^{2+}{}_{\mathrm{cyt}}]_{\mathrm{free}}}{dt} = f(\lambda I_{\mathrm{Ca}} + k_{\mathrm{exch}}\left([Ca^{2+}{}_{\mathrm{ER}}]_{\mathrm{free}} \pm [Ca^{2+}{}_{\mathrm{cyt}}]_{\mathrm{free}}\right) \pm k_{\mathrm{Ca}}[Ca^{2+}{}_{\mathrm{cyt}}]_{\mathrm{free}}). \quad (9)$$

In Eq. 9, f denotes the fixed ratio of free Ca^{2+} to total Ca^{2+}. In Eq. 9, only concentrations of free Ca^{2+} are used to determine total Ca^{2+} fluxes between compartments or out of the cell because bound Ca^{2+} is generally not transported across membranes.

From Eq. 9, it follows that the effect of a small ratio f is to greatly slow down the rate of change of Ca^{2+} concentration. As a result, $[Ca^{2+}{}_{\mathrm{cyt}}]_{\mathrm{free}}$ can become one of the slowest changing variables in models of electrical activity in neurons. With these models, oscillations in $[Ca^{2+}{}_{\mathrm{cyt\#}}\mathrm{cb}_{\mathrm{free}}$ with a period on the order of seconds can be simulated. These oscillations are often coupled to oscillations of the membrane potential, and sometimes bursts of action potentials are superimposed on the membrane potential oscillations (Amini *et al.*, 1999; Canavier *et al.*, 1993; Smolen and Keizer, 1992).

When modeling diffusion of ions other than Ca^{2+}, or of small molecules, including buffering is often less important because there are fewer binding sites than for Ca^{2+}. For modeling the diffusion of macromolecules, it is desirable to include buffering. However, there are usually insufficient data to determine the number and distribution of binding sites for specific macromolecules. With this limitation, a reasonable approach is to guess a plausible value for the macromolecular diffusion coefficient and then simulate experiments that measure macromolecular movement rates. A common experimental technique is ***fluorescence recovery after photobleaching*** (FRAP) (Kaufman and Jain, 1990). This technique uses strong brief illumination of an intracellular region with a laser. The laser eliminates emission from a fluorescently tagged macromolecule within the region by photobleaching the fluorophore. Afterward, the time course of fluorescence recovery is monitored as macromolecule diffuses in from other regions. Fitting this time course with computer simulations provides an estimate for the diffusion coefficient.

Active Transport May Dominate over Diffusion for Macromolecules

For most macromolecules, intracellular movement is often via ***active transport*** requiring ATP. Active transport is especially important in cells with extended morphologies, such as neurons. In neurons, calculations indicate that passive diffusion of mRNAs and proteins from the soma into narrow dendrites would be much slower than the observed rates of movement (Sabry *et al.*, 1995). Active transport consists of directed movement along cytoskeletal elements of specific macromolecules or of small, membrane-bound vesicles containing macromolecules. The movement is mediated by motor proteins such as kinesin and dynein. Active transport has not been modeled as often as diffusion. For constraining models of active macromolecular transport, data specific to neurons need to be used because there is great variability in transport rates between neurons and other cell types. A reasonable approximation is to assume a constant drift of macromolecule, at a velocity that may vary between different regions of a neuron. If diffusive movement is also important, it should be modeled separately. As a first approximation, diffusion might be simply added to the motion due to active transport, providing an additional random motion. Diffusion might be ignored if data suggest active transport is much more important for particular macromolecules. As mentioned above, this appears to be the case for transport of many RNAs and proteins into extended neuronal processes.

Standard Equations Simplify Modeling of Enzymatic Reactions, Feedback Loops, and Allosteric Interactions

In cells, most biochemical reactions of interest are catalyzed by enzymes, and a variety of mathematical descriptions have been developed for these reactions. Many enzymatic reactions have complex kinetic mechanisms, and specialized equations are needed to describe their rates in detail (Segel, 1975). When a series or group of reactions is being modeled, however, it is more common to use simplified equations for the individual reaction rates. A few such forms have become standard.

To review these equations, it is first helpful to review the definition of ***reaction order***. A zero-order reaction converts substrate into product at a fixed rate independent of substrate concentration. A first-order reaction converts substrate into product at a rate proportional to substrate concentration. A second-order reaction creates product at a rate proportional to either the product of two substrate concentrations or the square of a single substrate concentration. Higher-order reactions are similarly defined. In many cases, an enzyme transforms a single substrate, S, into a single product, P. The simplest assumption is that the rate of production of P is first-order with respect to S. This assumption can be useful when many reactions are being modeled, to minimize the complexity of the model and the computational time required for simulations (Bhalla and Iyengar, 1999). The next level of detail considers ***saturation*** of the enzymatic reaction rate at high concentrations of S. Then, the reaction no longer has a definite order, and a nonlinear equation must be used for the rate. The simplest such equation for the rate of production of P, $d[\mathrm{P}]/dt$, is the standard ***Michaelis–Menten equation***:

$$\frac{d[P]}{dt} = \frac{V_{\max}[S]}{[S] + K_{\mathrm{m}}}. \tag{10}$$

This equation has been found *in vitro* to accurately describe the rates of many enzymatic reactions. $V_{\max}$ represents the maximal enzyme velocity when it is fully saturated with the substrate S, and K_{m} represents the concentration of S at which the velocity is half of its maximal value. Note that if the enzyme is saturated with substrate (high [S]), Eq. 10 reduces to a description of a zero-order reaction.

If two substrates S_1 and S_2 are converted into a single product P, then the simplest assumption is that the rate of production of P is second-order, proportional to the product $[S_1]\,[S_2]$. One can add more realism by including saturation effects. This can be done by using a product of Michaelis–Menten expressions. Suppose also a first-order degradation of P. Then a differential equation for the *in vivo* rate of change of the concentration of P is

$$\frac{d[P]}{dt} = k_{\max}\left(\frac{[S_1]}{[S_1] + K_1}\frac{[S_2]}{[S_2] + K_2}\right) \pm k_{\mathrm{deg}}[P]. \tag{11}$$

Here, the first term on the right-hand side is a product of Michaelis–Menten expressions for $[S_1]$ and $[S_2]$. The maximal velocities $V_{\max}$ have been combined into the parameter $k_{\max}$. The second term represents first-order degradation. In Eq. 11, K_1, K_2, $k_{\max}$, and k_{deg} are parameters to be estimated from experimental data.

A model of a biochemical reaction pathway is composed of a set of differential equations such as Eq. 11. There is an equation for the rate of change of the concentration of each reaction substrate and product. Given initial values for the concentrations of all biochemical species, numerical integration of the differential equations is done in the manner described

previously for Eq. 1. The integration gives values of the concentrations for times subsequent to the initial time.

Allosteric Interactions between Enzymes and Small Molecules Can Alter Enzyme Activities and Mediate Feedback

Binding of small molecules can alter an enzyme's conformation and alter the rate of the reaction catalyzed by the enzyme. Often, such allosteric interactions are with effector molecules not involved in the reaction. But for some enzymes (*e.g.*, pyruvate kinase, phosphofructokinase) substrates or products can serve as allosteric effectors. Allosteric interactions can therefore mediate feedback and feedforward interactions within a biochemical pathway, as well as crosstalk between pathways.

In a ***feedback interaction***, a product of an enzymatic reaction affects the activity of another enzyme earlier in the pathway, whereas in a ***feedforward interaction***, the affected enzyme is later in the pathway. With ***cross-talk***, a metabolite from one pathway affects the activity of an enzyme in another pathway. Two types of feedback can be distinguished. If the product of a later reaction acts to speed up an earlier reaction, the feedback is positive; if the effect is to slow down the earlier reaction, the feedback is negative. Positive feedback tends to drive a biochemical pathway to a state of maximal activity determined by the saturated rate of the slowest individual reaction, whereas negative feedback tends to drive the pathway to a state of low activity. Graphically, such an interaction is often represented as in Fig. 14.2A, where the circled minus sign denotes negative feedback.

In models of enzyme regulation, allosteric interactions are commonly represented by ***Hill functions*** (Segel, 1975). These are saturable functions of the concentration of the effector molecule. With the concentration of effector denoted by [L], if [L] activates an enzyme, the enzyme activity is taken as proportional to the following increasing function of the nth power of [L]:

$$\frac{[L]^n}{[L]^n + K_H^n}. \tag{12a}$$

When the Hill function of Eq. 12a is plotted versus effector concentration [L], the graph has a characteristic sigmoid shape. The enzyme activity is near 0 for low values of [L]. In Eq. 12a, the parameter K^n_H has units of concentration. When [L] = K^n_H, the activity has a value of 0.5. Over a range of [L] centered about K^n_H, the activity increases rather steeply to near its maximal value of one. The parameter n is called the Hill coefficient. Greater values of n correspond to steeper sigmoids, that is, to a narrowing of the range of [L] over which the enzyme activity is significantly above 0 and also significantly below 1.

If L inhibits an enzyme, the enzyme activity is taken as proportional to a decreasing function of [L]:

$$\frac{K_H^n}{[L]^n + K_H^n}. \tag{12b}$$

In Eq. 12b, the parameters n and K^n_H have the same meanings as in Eq. 12a. As an example of how these functions are used in rate equations for biochemical reactions, inclusion of an increasing Hill function in Eq. 11 gives

$$\frac{d[P]}{dt}\left(\frac{[L]^n}{[L]^n + K_H^n}\right)\frac{V_{max}[S]}{[S] + K_m}. \tag{13}$$

Often, an enzyme has multiple binding sites for an allosteric effector, particularly if the enzyme is composed of multiple subunits. Greater values of the Hill coefficient often correspond to a larger number of binding sites for a given allosteric effector. Indeed, experimentally determined Hill coefficients are often taken as a rough indication of the number of binding sites. Instead of Hill functions, more complex expressions based on ***Monod–Wyman–Changeux allosteric theory***, or similar theories, are sometimes used (Segel, 1975).

Figure 14.2B illustrates a relatively simple model (Cooper *et al.*, 1995) that incorporates Hill functions, reaction rates directly proportional to substrate concentration, and first-order degradation. This model describes the relationship between cyclic AMP (cAMP) production and the rate of Ca^{2+} influx into a cell. The model can simulate persistent oscillations in [cAMP] if the parameter values fall within the proper range (legend to Fig. 14.2).

The model contains four biochemical species: cAMP, Ca^{2+}, active adenylyl cyclase enzyme (denoted by AC), and active Ca^{2+} channels in the plasma membrane (denoted by Y). Some model species alter the production or degradation rates of others (Fig. 14.2B). The rate of cAMP production is assumed to be proportional to the amount of active adenylyl cyclase enzyme. cAMP is assumed to be degraded by a first-order process. Therefore, the differential equation describing the rate of change of cAMP concentration is

$$\frac{d[\text{cAMP}]}{dt} = k_1[\text{AC}] \pm k_2[\text{cAMP}]. \tag{14}$$

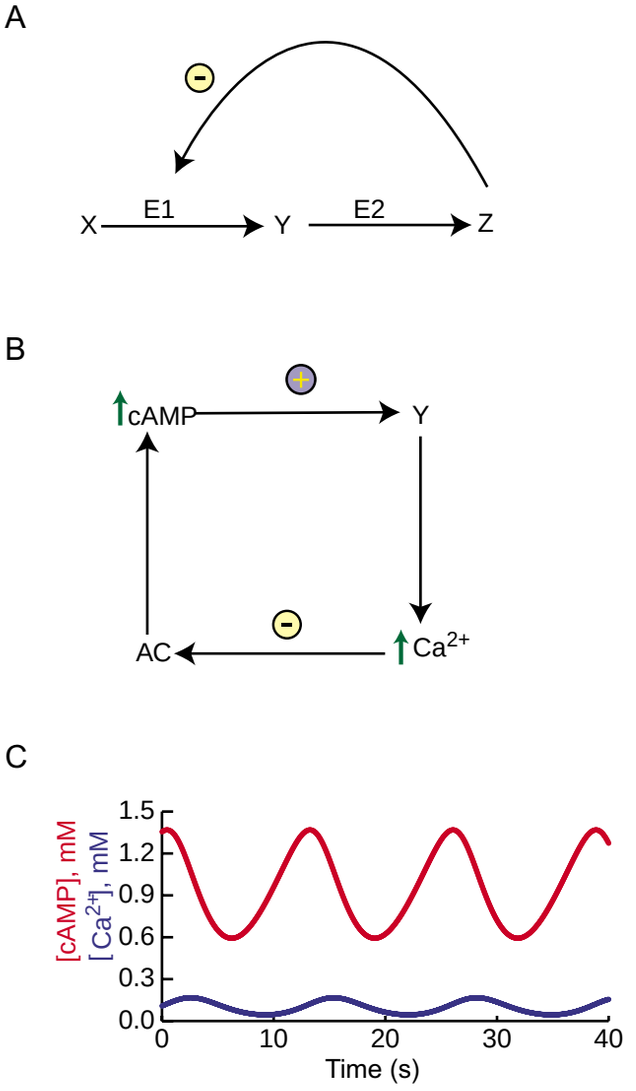

FIGURE 14.2 Feedback within two model signaling pathways. (A) Negative feedback within a simple, linear reaction scheme. Metabolite X is transformed into Y which is transformed into end product Z. Z inhibits the enzyme E1 that catalyzes the X → Y reaction. (B) A model that captures some relationships between cAMP production and Ca^{2+} influx. cAMP activates Ca^{2+} channels (denoted *Y*). Ca^{2+} influx is thereby increased. Ca^{2+} influx inhibits adenylyl cyclase (AC). The overall effect is a negative-feedback loop in which cAMP inhibits its own production. (C) Oscillations in cAMP and Ca^{2+} are sustained by the negative-feedback loop. For this simulation, the values of the parameters in Eqs. 14–17 are $k_1 = 1.0\ s^{-1}$, $k_2 = 0.5\ s^{-1}$, $k_3 = 1.0 s^{-1}$, $k_4 = 0.5\ s^{-1}$, $k_5 = 0.45\ \mu M\ s^{-1}$, $k_6 = 1.0\ s^{-1}$, $k_7 = 0.11\ s^{-1}$, $k_8 = 2.0\ \mu M\ s^{-1}$, $K_1 = 2.0\ \mu M$, $K_2 = 0.2\ \mu M$. Initial values for the model variables at $t = 0$ are cAMP = 1.0 μM, AC = 0.5 μM, $Y = 0.05\ \mu M$, and $Ca^{2+} = 0.1\ \mu M$.

The rate of Ca^{2+} influx is assumed to be proportional to the number of active Ca^{2+} channels in the plasma membrane. Ca^{2+} is extruded from the cell by a first-order process. Therefore, for the rate of change of Ca^{2+} concentration,

$$\frac{d[Ca^{2+}]}{dt} = k_3 Y \pm k_4\left[Ca^{2+}\right], \tag{15}$$

Ca^{2+} channels are assumed to be activated by the binding of cAMP. A Hill function, with a Hill coefficient of 3, characterizes activation by cAMP. Channels deactivate in a first-order fashion in the absence of cAMP. By use of Eq. 12a, the differential equation for the number of active channels, denoted *Y*, can be written as

$$\frac{dy}{dt} = \frac{k_5[\text{cAMP}]^3}{[\text{cAMP}]^3 + K_1{}^3} \pm k_6 Y. \tag{16}$$

Ca^{2+} is assumed to inhibit adenylyl cyclase. Mathematically, this inhibition can be represented by an equation in which Ca^{2+} increases the rate at which the variable AC decreases. This effect of Ca^{2+} can be described by a Hill function. The resulting differential equation for AC is

$$\frac{d\,\text{AC}}{dt} = k_7 \pm \text{AC}\frac{k_8\left[\text{Ca}^{2+}\right]^3}{\left[\text{Ca}^{2+}\right]^3 + K_2{}^3}. \tag{17}$$

As discussed in Chapter 12, the actual regulation of adenylyl cyclase is more complex than embodied in Eq. 17. Some neuronal isoforms of adenylyl cyclase are inhibited by elevations of Ca^{2+} such as occur during electrical activity, but others are stimulated (Chapters 12 and 18).

If Hill coefficients greater than 2 are chosen in Eqs. 16 and 17, the model can produce stable oscillations in [cAMP] and the other variables (Fig. 14.2C). The generation of oscillations by this model requires a negative-feedback loop. This operates as follows. An initial increase in the level of cAMP activates Ca^{2+} channels, allowing the influx of Ca^{2+}. Ca^{2+}, in turn, inhibits adenylyl cyclase. The inhibition acts to decrease the concentration of cAMP, closing the loop. The model helps to suggest a principle that negative-feedback loops favor the occurrence of oscillations in concentrations and reaction rates.

Positive and Negative Feedback Can Support Complex Dynamics of Biochemical Pathways

Feedback Can Sustain Oscillations or Multistability of Concentrations and Reaction Rates

One interesting behavior in biochemical pathways is ***persistent oscillations*** in the rates of enzymatic reactions and in the concentrations of substrates and products. For example, oscillations have been observed in the metabolic flux through glycolysis and also in the rates of secretion of hormones such as

insulin. The previous section discussed a model (Fig. 2) in which concentration oscillations were driven by a negative-feedback loop. More generally, oscillations in reaction rates and concentrations commonly rely, on negative feedback to sustain oscillations (Gartner, 1990). Models of biochemical systems that rely on positive feedback tend to display another type of complex behavior. This behavior, termed ***multistability***, is defined as the existence of multiple steady states for the concentrations of the chemical species. Each state is fixed in time and corresponds to a fixed metabolic flux through the pathway. Each state is stable in that small disturbances of the system die out with time so that the system, if originally in one of the states, returns to that state. Large disturbances of the system, however, can switch it between stable states.

Bistability is a specific type of multistability with two stable states. Bistability was discussed in Chapter 7 (Fig. 7.19) in the context of a model neuron that could exhibit a fixed, stable membrane potential but, following a brief current injection, would switch to a state of continuous electrical spiking. ***Ca^{2+}***/calmodulin-activated protein kinase II (***CAMKII***) activity may provide an example of biochemical bistability relevant to learning and memory. As discussed in Chapter 12, CAMKII exists *in vivo* as a holoenzyme of multiple subunits (~12). CAMKII is activated by binding of Ca^{2+}-calmodulin complexes to the subunits. Each subunit of CAMKII can be phosphorylated on Thr-286. The enzymatic activity of a phosphorylated subunit is increased, and this activity persists when Ca^{2+}-calmodulin is not bound to the subunit. A holoenzyme can undergo ***autophosphorylation*** in which active subunits phosphorylate other subunits that have Ca^{2+}-calmodulin complexes bound (Hanson *et al.*, 1994; Zhabotinsky, 2000). Elevations of Ca^{2+} increase the fraction of calmodulin saturated with bound Ca^{2+} and thereby increase the frequency of CAMKII autophosphorylation reactions. Modeling has suggested that CAMKII might act as a ***bistable switch*** (Zhabotinsky, 2000; Lisman and Zhabotinsky, 2001). For a given CAMKII holoenzyme, if a brief electrical stimulus caused Ca^{2+} influx that phosphorylated a critical number of subunits on Thr-286, then these subunits might phosphorylate the remaining subunits. Then the holoenzyme would remain active after Ca^{2+} influx ceased. As mentioned in Chapters 12 and 18, prolonged activation of CAMKII may be important for long-term synaptic potentiation in response to correlated pre- and postsynaptic electrical activity (Lisman, 1994). Such synaptic strengthening, in turn, appears essential for the formation of long-term memories (Martin *et al.*, 2000).

The most recent models (Zhabotinsky, 2000; Lisman and Zhabotinsky, 2001; Lisman, 1994) suggest that CAMKII could remain highly active and autophosphorylated only in the postsynaptic regions of dendrites. In other regions of the cytosol, the total concentration of CAMKII is much lower relative to phosphatases that counter the autophosphorylation reaction, so the autophosphorylated state of CAMKII could not be maintained after $[Ca^{2+}]$ returned to its rest level. Thus, in the postsynaptic region, CAMKII might act as a bistable switch in which a brief influx of Ca^{2+} would lead to long-term activation of CAMKII via sustained autophosphorylation. Figure 14.3A shows schematically the autophosphorylation process, and Fig. 14.3B illustrates how bistable activity of the CAMKII holoenzyme can be represented as a plot of enzyme activity versus $[Ca^{2+}]$.

Chapter 7 introduced the concept of a ***bifurcation diagram***, in which the stable or unstable steady states of a variable in a model are plotted. The plot shows how the steady states change as a function of a model parameter. For example, in a model of neuronal excitability, a stable solution for membrane potential changes its value and perhaps loses stability if a conductance parameter or a background stimulus current is varied (see Figs. 7.18 and 7.20). Figure 14.3B is a bifurcation diagram showing how the activity of CAMKII varies as $[Ca^{2+}]$ is varied. The solid (upper and lower) portions of the black curve give the values of CAMKII activity that are stable at any given $[Ca^{2+}]$. If $[Ca^{2+}]$ lies within the blue region, there are two possible values of CAMKII activity. The higher activity corresponds to a higher degree of CAMKII autophosphorylation. The dashed portion of the black curve corresponds to an intermediate activity that is unstable: a small change in $[Ca^{2+}]$ will cause CAMKII activity to move up or down to one of the two stable states. Prior to a stimulus that leads to an increase in Ca^{2+} influx, the point representing the state of CAMKII might lie in the lower steady state of the graph—low activity, at a low (resting) level of $[Ca^{2+}]$. This state is labeled 1. Electrical activity and consequent Ca^{2+} influx can move the Ca^{2+} concentration well to the right, from point 1 on the low steady state to point 2, where the lower steady state of CAMKII activity no longer exists. At point 2 only the state of high CAMKII activity is stable. If $[Ca^{2+}]$ stays above the blue region for some critical time, Ca^{2+}-calmodulin—induced autophosphorylation will move the activity of CAMKII up to a high value, to point 3. Then, when Ca^{2+} concentration returns to a lower level, the state of CAMKII moves back to the left, to point 4. But the CAMKII activity still remains on the upper portion of the curve—high activity, with sustained autophosphorylation.

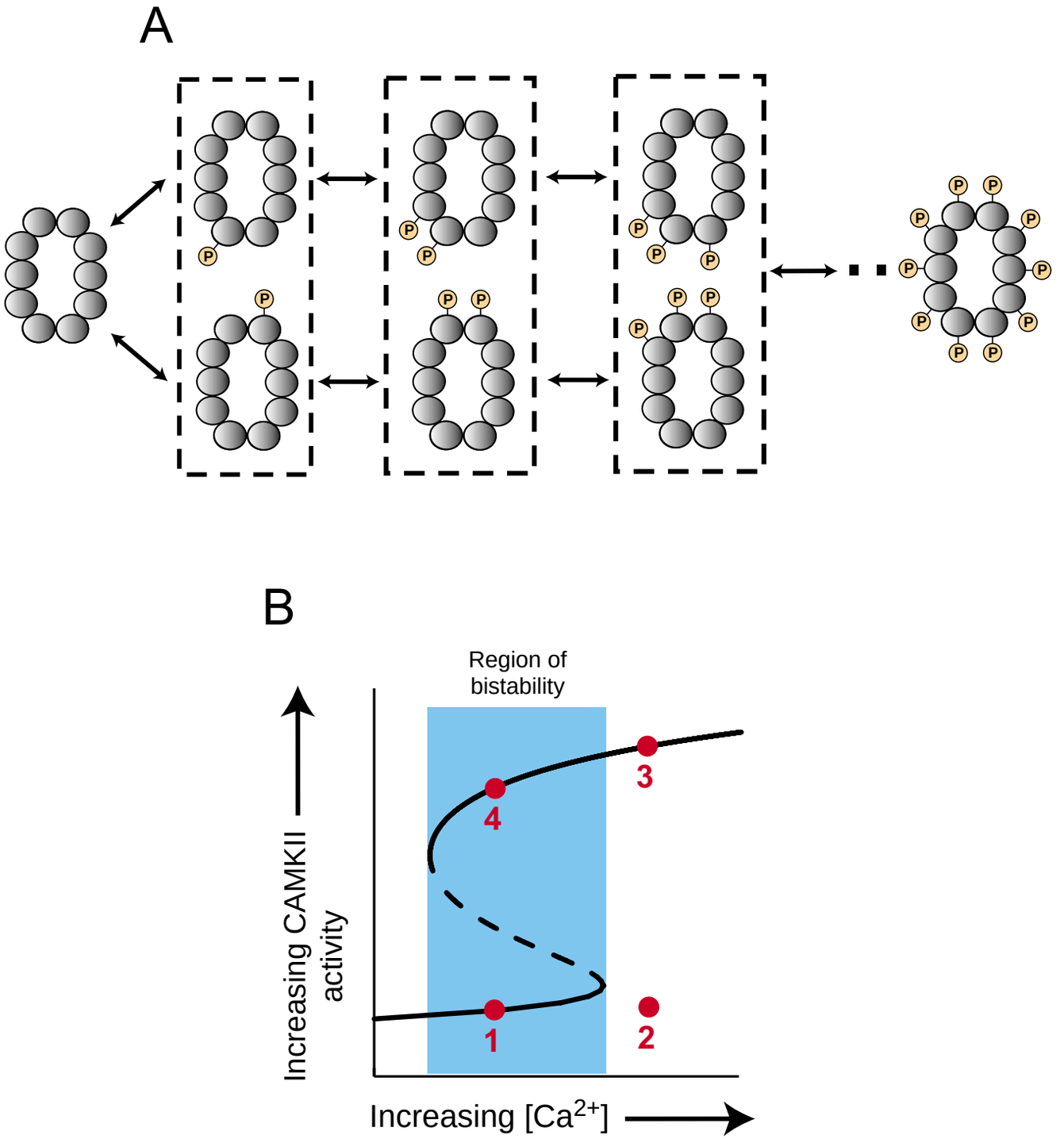

FIGURE 14.3 Autophosphorylation of CAMKII may lead to bistability in enzyme activity. (A) Schematic illustrating multiple phosphorylation states. If it is assumed that there are 10 subunits per holoenzyme, there are a large number of possible states, but if CAMKII activity depends only on the number of phosphorylated subunits and not their location within the holoenzyme, there are only 11 states of differing enzyme activity. Five of these states are shown, corresponding to 0, 1, 2, 3, and 10 phosphorylated subunits. Phosphate groups are orange. A calmodulin molecule with bound Ca^{2+} (not shown) must be bound to a subunit for phosphorylation to be possible. (B) Schematic illustrating bistability. The *x* axis represents intracellular Ca^{2+} concentration. For a range of Ca^{2+} concentrations, there is both a low and a high stable steady state for CAMKII activity (solid portions of curve, blue region of graph). The two stable states are separated by an unstable steady state (dashed portion of curve).

An important caveat is in order regarding the significance of the bistability in Fig. 14.3. Long-lasting changes in CAMKII activity have not yet been shown to be important for long-term synaptic potentiation (LTP). Autophosphorylation of CAMKII does occur after electrical stimuli that produce LTP (Yamagata and Obata, 1998; Ouyang *et al.*, 1997). When autophosphorylation is prevented by mutating Thr-286, LTP *induction* is severely impaired (Giese *et al.*, 1998). However, even if CAMKII autophosphorylation and increased activity are long-lasting, the increased activity may not be required for LTP *maintenance*. Inhibitors of CAMKII applied subsequent to LTP induction are most often reported not to affect LTP maintenance (Chen *et al.*, 2001).

Negative or positive feedback due to allosteric regulation of enzymes can generate oscillations in the rate of metabolic flux through a biochemical pathway. The best known example is oscillations in the rate of glycolysis. The enzyme phosphofructokinase (PFK) is largely responsible for glycolytic oscillations in a variety of experimental preparations. Sustained oscillations have been found in several systems, for example, in suspended yeast cells (Dano *et al.*, 1999). Glycolytic oscillations may modulate the electrical activity of some excitable cells (Prentki *et al.*, 1997). PFK is activated by one of its reaction products, adenosine diphosphate (ADP). The activation is cooperative, depending on the second or higher power of ADP concentration. Thus, positive feedback occurs, with production of ADP progressively activating PFK until PFK activity and ADP concentration plateau at high levels. No negative feedback is present. Usually, positive feedback alone cannot support oscillations. In glycolysis, however, the substrate of PFK (fructose 6-phosphate) is supplied at a limited rate. Therefore, cycles of substrate depletion can occur. When ADP concentration and PFK activity are high, the substrate of PFK is used faster than it is supplied. A fall in the substrate concentration leads to a drop in the production of ADP and a loss of PFK activity. PFK activity then remains low while substrate accumulates again. Eventually, substrate accumulation raises the rate of production of ADP, and enough ADP is formed to reach the threshold for positive feedback to become effective. Then the cycle can begin anew. Cooperativity of activation of PFK by ADP is essential for these oscillations. Several mathematical models have been developed that describe these oscillations (Goldbeter, 1996). With these models, bistability in PFK activity can also appear when different values of kinetic parameters are assumed. This result is as expected, since bistability is typical for models with positive feedback.

Several Mechanisms, Including Positive Feedback, Can Yield High Sensitivity of Response Magnitude to Signal Strength

The term ***ultrasensitivity*** refers to the following phenomenon. Sometimes a modest change in the concentration of substrate of an enzyme, or a modest change in the activity of an enzyme, greatly changes the net rate of the reaction catalyzed by that enzyme. For example, in a biochemical pathway, a relatively abrupt transition in metabolic flux from near zero to near maximum might be seen in response to a modest change in the concentration of the substrate of the first reaction in the pathway. Such switchlike behavior can be generated by several mechanisms. One mechanism relies on allosteric binding of a substrate to multiple sites on an enzyme in a cooperative fashion, such as that described by Eq. 12a. If the Hill coefficient of cooperativity is high (*i.e.*, high n in Eq. 12a), then a small change in substrate level can yield a large change in enzyme activity. A second mechanism is ***zero-order ultrasensitivity*** (Goldbeter and Koshland, 1984). Here, two enzymes catalyze the same biochemical transformation, one in the forward direction and the other in the reverse direction. The enzyme pair could be a kinase and a phosphatase. Both enzymes must be nearly saturated with substrate, so that both the reverse and forward reactions are approximately zero-order. Then the rates of these reactions hardly change with the concentrations of their substrates. At steady state, the substrate concentrations are often such that the rates of both reactions are nearly equal. Then the net flux, or the difference between the rates of the forward and reverse reactions, is much smaller than the rates of the individual reactions. Now, suppose there is a small increase in the activity (V_{max}) of the enzyme catalyzing the forward reaction. This unbalances the rates so that the forward reaction is faster. Since this enzyme is saturated with substrate, a large drop in the concentration of substrate is required to bring the rates back into balance. Thus, a small change in enzyme activity results in a large change in the ratio of substrate to product.

A well-known signaling pathway in which zero-order ultrasensitivity may be important begins with hormonal or neurotransmitter receptors and continues through activation of several protein kinases to affect the activity of one or more isoforms of mitogen-activated protein kinase (MAPK) (Fig. 14.4A). In this pathway, MAPK is itself a substrate for a kinase termed mitogen-activated protein kinase kinase (MAPKK or MEK), and MAPKK is in turn a substrate for MAP kinase kinase kinase (MAPKKK). Phosphorylation of MAPK by MAPKK is necessary for MAPK activation. Some isoforms of MAPK may

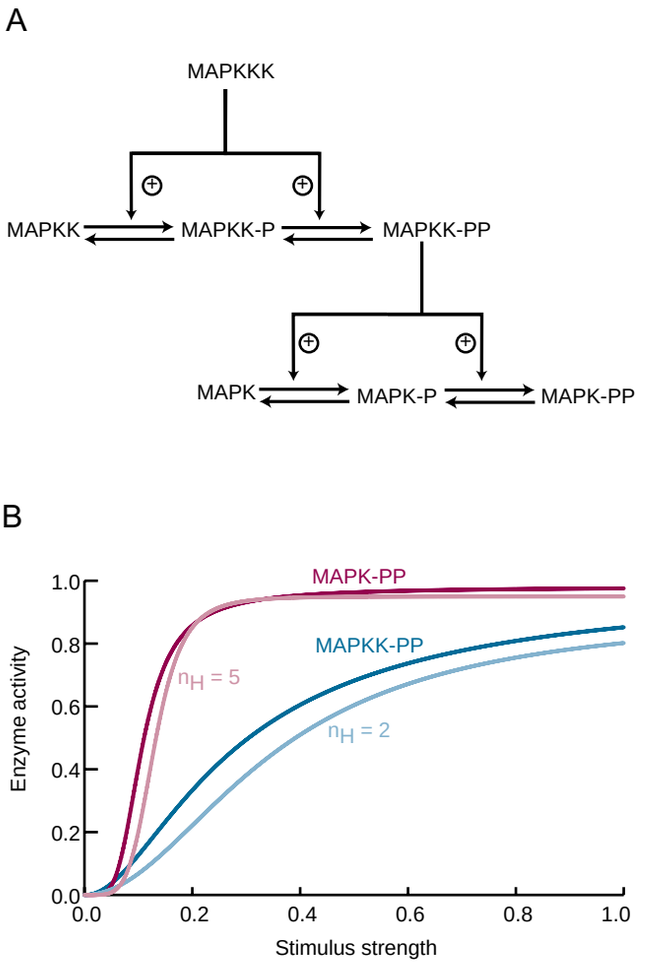

FIGURE 14.4 A mechanism for generating ultrasensitivity in the stimulus–response curve of a MAP kinase signaling cascade. (A) Kinetic scheme illustrating double phosphorylations of both MAPKK and MAPK. Phosphorylations are reversible. (B) Stimulus–response curves for the activities of MAPK (top, red curve) and MAPKK (dark green curve) based on the kinetic scheme of (A). For both enzymes, the activity is assumed proportional to the fraction that is doubly phosphorylated. The stimulus is a constant level of MAPKKK activation. Also plotted, alongside the stimulus–response curves, are graphs of Hill functions generated using Eq. 12a. For the brown curve, the Hill coefficient n_H is 5; this curve is similar to the stimulus–response curve of MAPK. For the blue curve, the Hill coefficient n_H is 2; this curve is similar to the stimulus–response curve of MAPKK.

be present in high enough concentrations to nearly saturate MAPKK. It has therefore been suggested that a small increase in the activity of MAPKK could cause, via zero-order ultrasensitivity, a large increase in phosphorylated and active MAPK. Modeling has suggested this occurs under physiological conditions (Ferrell, 1996; Huang and Ferrell, 1996).

In addition to zero-order ultrasensitivity, the MAPK pathway may exhibit ultrasensitivity as a result of a requirement for multiple phosphorylations of MAPK and MAPKK (Ferrell, 1996). MAPK must be doubly phosphorylated by MAPKK to be activated. In turn, to be activated, MAPKK must also be doubly phosphorylated by MAPKKK. The phosphorylations are reversible, and the phosphatase activities are often considered to be constant (Huang and Ferrell, 1996). Figure 14.4B illustrates stimulus–response curves for the doubly phosphorylated fractions of MAPK, and MAPKK versus the strength of an input stimulus. These curves were calculated from a model (Huang and Ferrell, 1996) that uses the kinetic scheme of Fig. 14.4A. The stimulus corresponds to a fixed activation level of MAPKKK in Fig. 14.4A. The stimulus was assumed to be applied long enough that all reactions in Fig. 14.4A attained equilibrium. The rates of change of the amounts of active enzymes can therefore be set equal to zero. The resulting system of equations can be solved to yield the fractions of doubly phosphorylated MAPKK and MAPK as a function of input stimulus strength. Figure 14.4B shows that the steep curve for MAPK phosphorylation can be approximately reproduced by Eq. 12a with a high Hill coefficient (~ 5). To use this equation, effector concentration is replaced by input stimulus strength. The curve for MAPKK phosphorylation is less steep (Hill coefficient of ~2).

Cross-Talk between Neuronal Signaling Pathways May Influence Stimulus-Induced Synaptic Changes

Electrical activity or exposure to neurotransmitters or growth factors can simultaneously activate a variety of signaling pathways in neurons. **Cross-talk** between pathways can be mediated by a chemical species that is produced or consumed by reactions in two pathways. Cross-talk can also be mediated by a species produced in one pathway that interacts allosterically with an enzyme in another pathway. Modeling of pathways can help identify points of possible cross-talk and ranges of parameter values that would make this cross-talk significant. Experiments could then examine whether parameter values fall in these ranges and whether cross-talk causes observable effects on system behavior.

One recent study (Bhalla and Iyengar, 1999) modeled glutamate-activated signaling, which involved activation of four signaling pathways at dendritic synapses of hippocampal pyramidal neurons. These signaling pathways activate protein kinase A (PKA), protein kinase C (PKC), MAPK, and CAMKII. Figure 14.5 illustrates points of cross-talk between these pathways. Experimental values for

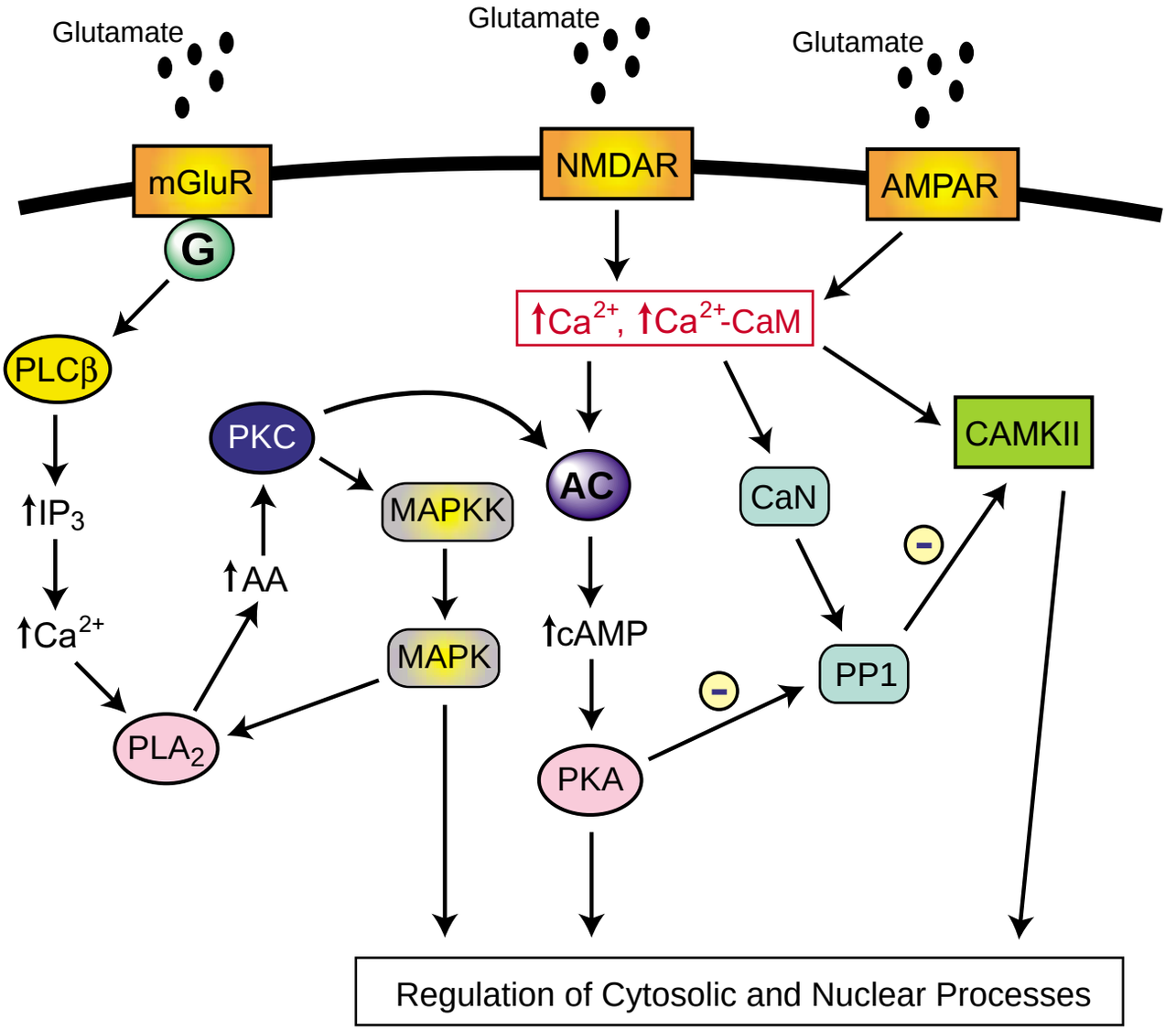

FIGURE 14.5 Aspects of a model that relates glutamate exposure at hippocampal synapses to long-term synaptic strengthening. Glutamate can act through metabotropic glutamate receptors (mGluR) to activate G proteins (G). Glutamate also acts through NMDA and AMPA receptors to increase intracellular levels of free Ca^{2+} and Ca^{2+} bound to calmodulin. These events lead to activation of phospholipase C (PLC), CAMKII, calcineurin (CaN), adenylyl cyclase (AC), and PKA. Two forms of cross-talk between these signaling pathways are illustrated. As discussed in the text, PKA activation leads to the inhibition of PP1. This inhibition relieves dephosphorylation of CAMKII by PP1, thus helping to sustain CAMKII activity. Also, MAPK activates phospholipase A_2 (PLA_2) and the resulting increase in arachidonic acid activates PKC. PKC in turn activates MAPKK, which further activates MAPK. As illustrated MAPK, PKA, and CAMKII regulate gene expression and cytosolic components, such as the cytoskeleton, that are essential for long-term synaptic strengthening.

model parameters were sometimes not available for neurons, so values from other cell types had to be used in this model. Despite this disadvantage, the model is useful for suggesting points of cross-talk. One possibility is a ***positive-feedback loop*** that increases both MAPK and PKC activity. MAPK can phosphorylate and activate the enzyme phospholipase A_2, whose activity generates the second messenger arachidonic acid (AA). AA activates PKC. In turn, PKC can phosphorylate and activate a guanine nucleotide exchange factor, which then activates Ras GTPase. Ras can then further activate the MAPK signaling cascade, closing the positive-feedback loop. In simulations with the model, a brief glutamate expo-

sure activated the positive-feedback loop. This caused the model to switch from a stable state with a low, basal activity of MAPK and PKC to a stable state with a high activity of both enzymes. In neurons, induction by glutamate of a prolonged activation of MAPK and PKC might correspond to induction of a large change in synaptic strength, dependent on a long-lasting phosphorylation by MAPK or PKC of transcription factors such as Ca^{2+}/cAMP—responsive element-binding protein (CREB).

A second point of possible cross-talk is a ***gate*** involving cAMP and CAMKII. As discussed above, autophosphorylation of CAMKII after a brief influx of Ca^{2+} might convert CAMKII to a long-lasting, active state independent of Ca^{2+}. Such a state might be essential for long-term potentiation of synapses. However, Ca^{2+} influx also elevates the concentration of Ca^{2+}-calmodulin complex, which in turn may activate a phosphatase, protein phosphatase I (PP1) (Bhalla and Iyengar, 1999). PP1 can dephosphorylate CAMKII. If cAMP levels are also elevated by the same stimulus that causes Ca^{2+} influx, the autophosphorylation of CAMKII might have a greater chance of becoming self-sustaining. This is because cAMP activates PKA, which in turn leads to inhibition of PP1, thus "opening a gate" to allow a high level of CAMKII phosphorylation. This high level could be self-sustaining after cAMP and PP1 activity return to basal levels, because once a critical number of subunits in a CAMKII holoenzyme have been phosphorylated, autophosphorylation of the remaining subunits may be rapid enough to overcome the effects of PP1. Then, the holoenzyme will remain phosphorylated and active until eventual degradation.

Simulations (Bhalla and Iyengar, 1999) suggested that this "gate" could be important. Glutamate exposure led to a long-lasting increase in CAMKII activity only if PP1 was inhibited by PKA. In that case, only stimuli that increased both Ca^{2+} and cAMP past threshold levels were predicted to yield prolonged activation of CAMKII. Recent experiments (Brown *et al.*, 2000) have supported the importance of this dual threshold of Ca^{2+} and cAMP levels in determining the degree of synaptic modification in hippocampal neurons. Addition of a cAMP analog together with electrical stimulation was observed to yield strong activation of CAMKII. Neither stimulus alone could produce strong CAMKII activation. Furthermore, only the combination of electrical stimulation and cAMP analog could induce long-term synaptic potentiation.

The model of Fig. 14.5 also helps to order elements of signaling pathways in a set of cause–effect relationships. For example, Fig. 14.5 suggests that during the biochemical events following glutamate exposure, PKA activation lies "downstream" of both PKC and MAPK activation, but "upstream" of CAMKII activation.

The model of Fig. 14.5 can discriminate between stimulus patterns such as those known to produce long-term potentiation (LTP) and long-term depression (LTD) of synapses (Bhalla, 2002) (see also Chapter 18). To demonstrate discrimination between stimulus patterns, a ***compartmental model*** of a neuron was constructed, part of which is shown schematically in Fig. 14.6. The biochemical model (Fig. 14.5) was assumed to operate in the terminal (uppermost) compartment of the dendritic spine (Fig. 14.6). Stimulus patterns were modeled as pulses of Ca^{2+} influx into the spine, which activate enzymes such as MAPK (Fig. 14.5). The compartmental model provides a method for simulating Ca^{2+} diffusion between different portions of the spine (different compartments) and between the spine and the dendritic shaft. Within these small structures, Ca^{2+} diffusion plays an essential role in shaping Ca^{2+} concentration changes following stimulation. Therefore, Ca^{2+} diffusion must be included to model the activation of neuronal biochemical pathways. Diffusion between the cylindrical compartments is modeled with a variant of Eq. 4. A compartmental model can also simulate the spread of voltage changes between portions of a neuron (*e.g.*, action potentials).

Activation of the MAPK–PKC feedback loop was simulated following eight different stimulus patterns. One pattern used was three tetanic stimuli, each of 100 pulses at a frequency of 100 Hz, with 60 s between tetani; this pattern has been used experimentally to produce LTP. Another pattern was 900 s of 1-Hz pulses; this pattern has been used experimentally to produce LTD. Even at low stimulus amplitude (small pulses of Ca^{2+} influx), long-lasting activation of the MAPK–PKC feedback loop resulted from the "LTD-producing" 1-Hz stimulus pattern. The "LTP-producing" tetanic stimulus pattern was also effective, but at a higher amplitude.

In an extensive series of simulations, different model parameters, such as the extent of Ca^{2+} buffering, were varied. The order of selectivity among stimulus patterns was defined by the stimulus amplitudes required to activate the MAPK–PKC feedback loop. The "LTD-producing" 1-Hz pattern was usually first in order (lowest amplitude). However, among the seven other patterns, numerous changes in selectivity order were observed when parameters were varied. Therefore, these simulations illustrate that the biochemical parameters of neurons may play a key role in determining which stimulus patterns are most effective for altering synapses.

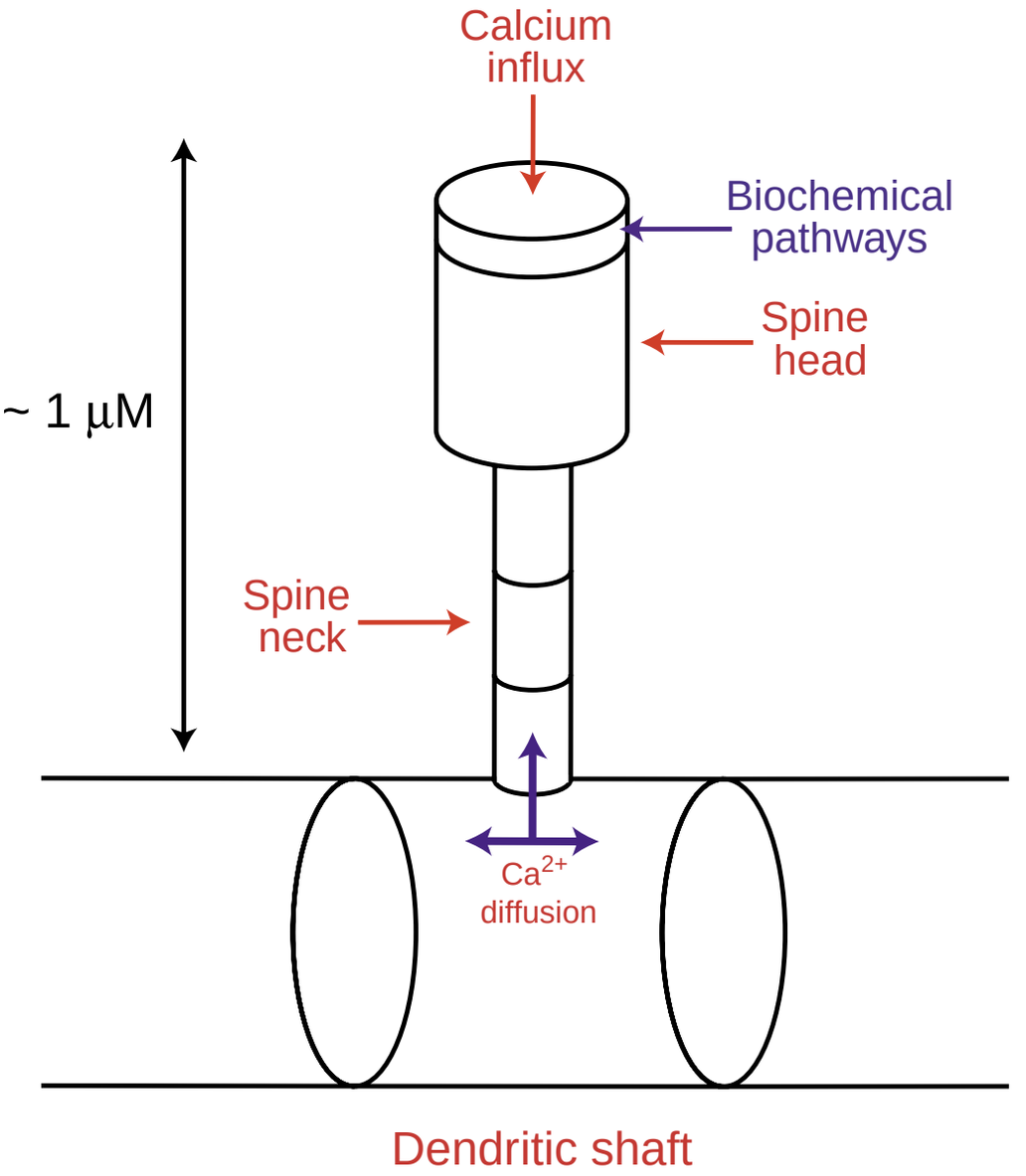

FIGURE 14.6 Part of a compartmental model of a hippocampal neuron. A dendritic spine and part of the dendritic shaft are shown. The spine head, the spine neck, and the dendritic shaft are each modeled as a series of cylindrical compartments. The compartments are necessary to model Ca^{2+} diffusion. Stimuli are modeled as pulses of Ca^{2+} influx into the spine. The components of the biochemical model of Fig. 14.5 are all assumed to exist in the terminal (uppermost) compartment of the spine. Ca^{2+} influx affects this model as discussed in the text, leading to activation of MAPK and other enzymes. MAPK activation can be prolonged via the positive feedback loop in which MAPK and PKC reciprocally activate each other (Fig. 14.5).

Before proceeding to discuss the methods of flux control analysis, stochastic modeling, and genetic modeling, it is important to address two general topics related to modeling biochemical systems. First, it is necessary to analyze how sensitive modeling results are to parameter values and to consider how experimental data constrain those values. Second, it is useful to develop the simplest model that can qualitatively reproduce the dynamics of a biochemical pathway. Starting with a complex model including multiple enzymes and metabolite concentrations, how might the number of variables be reduced while preserving a behavior of interest, such as oscillations in concentrations?

GENERAL ISSUES IN THE MODELING OF BIOCHEMICAL SYSTEMS

Analyzing Sensitivity of Model Behavior to Parameter Changes

It is necessary to assess the sensitivity of models to modest variations in the values of parameters. Genetic and biochemical systems are commonly observed to be robust even to large changes in the values of parameters, such as genetic mutations that alter enzyme activities (Wagner, 2000; Little *et al.*, 1999). The qualitative behavior of a gene network or biochemical pathway is often preserved due to evolved compensatory mechanisms. Therefore, models of these systems should most often not exhibit large variability in dynamics after small parameter changes. A standard method of assessing robustness to parameter changes is to define a set of sensitivities S_i, with the index i ranging over all model parameters p_i (Beck and Arnold, 1977; Frank, 1978). Let R denote the amplitude of the response of a signaling pathway to a fixed stimulus. For each p_i, a small change is made, and the resulting change in R is determined. The ***relative sensitivity*** S_i is then defined as the *relative*, or *fractional*, change in R divided by the *relative* change in p_i (Beck and Arnold, 1977, Frank, 1978)

$$S_i = \frac{\Delta R / R}{\Delta p_i / p_i}. \tag{18}$$

The relative sensitivity has the advantage that it is independent of the magnitudes and units of R and of the p_i.

R in Eq. 18 could also represent the time delay between a simulated stimulus and response, or the period of a simulated oscillation in gene transcription rate. In general, R is some quantity that has been measured and whose simulation is a major goal of model development.

The S_i in Eq. 18 are determined for small changes (10% or less) in the values of each individual parameter. For a model to be considered ***robust*** (*i.e.*, not overly sensitive) the S_i should not be too large. These values should generally not exceed ~10, unless there is experimental evidence that a response is particularly sensitive to a specific parameter. In practice, determinations of S_i or similar measures are complemented by qualitative assessments of whether particular behaviors (*e.g.*, oscillations in reaction rates) are preserved during modest parameter changes.

More detailed investigations vary multiple parameters simultaneously. The goal is to determine model behavior in regions of the multidimensional ***parameter space*** whose coordinate axes are the parameter values. For example, a region might support multiple stable solutions for metabolite concentrations and reaction rates, as does the blue region in Fig. 14.3B. Characterizing the location and size of such a region could predict that particular *in vivo* conditions would support multistability. However, a model of a biochemical pathway or of a network of co-regulated genes often has too many parameters to make a thorough characterization of the behavior in parameter space computationally feasible.

Bifurcation analysis (Wiggins, 1990; Rinzel, 1985) can help in determining and visualizing model behavior in parameter space. This technique allows determination of the curves or surfaces in parameter space at which model behavior undergoes significant changes. For example, with parameter values on one side of such a surface, the model variables may maintain a stable equilibrium. For parameter values on the other side of the surface, the equilibrium may disappear and persistent oscillations of model variables may appear. Software packages have been developed to determine and plot these curves or surfaces (Doedel, 1981).

Parameter Uncertainties Imply the Majority of Models are Qualitative, Not Quantitative, Descriptions

Models of biochemical pathways usually contain parameters whose values are not well constrained by experiment. It is obligatory for investigators to state which parameters in their models are poorly constrained, because parameter values might later be found to differ considerably from those used in a given model. Such differences could falsify the model because simulation of experimental results might no longer be possible.

Standard experiments can be done *in vitro* to estimate some parameter values. For example, enzyme Michaelis constants (*e.g.*, the parameters K_1 and K_2 in Eq. 11) are often estimated with preparations containing small amounts of enzyme. Other parameters are harder to estimate. For example, it is difficult to estimate the amount of active enzyme per cell. Therefore the maximal velocities of enzymes *in vivo* are often poorly constrained.

Many parameters such as reaction rate constants, enzyme activities, and Michaelis constants depend on the activity coefficients of enzymes and reactants. Activity coefficients are likely to be considerably dif-

ferent *in vivo* than *in vitro*. In cells, a high concentration of macromolecules creates a ***macromolecular crowding*** effect. Experiments with crowding by inert substances such as polyethylene glycol demonstrate that macromolecular crowding raises activity coefficients of all macromolecular species (Zimmerman and Minton, 1993). This increase in activities preferentially increases association rates and consequently increases levels of aggregates at the expense of monomers. For example, consider the association and dissociation rates, R_f and R_b, respectively, that govern the formation of an AB dimer from monomers of A and B:

$$R_f = k_f \lambda_A [A] \lambda_B [B], \tag{19a}$$

$$R_b = k_b \lambda_{AB} [AB]. \tag{19b}$$

In Eqs. 19a and 19b, k_f and k_b are standard rate constants. λ_A, λ_B, and λ_{AB}, are activity coefficients for A and B monomers and for the AB dimer. It is seen that the concentrations of A, B, and AB are each multiplied by the corresponding activity coefficients. The association rate R_f contains the product of two activity coefficients, so R_f tends to be enhanced more than R_b when activity coefficients are raised by macromolecular crowding. Therefore, formation of AB dimers is favored.

Increased association rates are expected to help stabilize signaling complexes containing multiple enzymes. This stabilization can enhance the efficacy of metabolite transfer between enzymes and, thereby, enhance the flux through a metabolic pathway (Rohwer *et al.*, 1998). The effect of macromolecular crowding on activity coefficients of small molecules is species-dependent: both charge and molecular weight are important.

Because of uncertainties in parameter values and activity coefficients, models of biochemical pathways should most commonly not be thought of as quantitative descriptions. Rather, they are most commonly qualitative descriptions. Simulations with such models are, as we have seen, very valuable for characterizing the types of dynamics likely to be supported by the biochemical architecture of a pathway. Also, simulations that adjust parameters to reproduce experimental results can help estimate the qualitative importance of interactions, such as feedback loops. Parameter adjustment could, for example, suggest that a dissociation constant for an allosteric effector is quite large and that, as a result, a feedback interaction mediated by that effector is weak. Further experiments are necessary to test such predictions.

Measurements of amounts of metabolites or second messengers after cell exposure to a hormone or neurotransmitter are particularly useful for estimating model parameter values. Groups of measurements are commonly taken at several time points following signaling pathway activation. Simulations of these experiments generally begin with reasonable "baseline" values for metabolite amounts. Then, the activity of key enzymes is temporarily increased to mimic the effect of the stimulus. An initial guess is made for model parameter values. The time courses of metabolite amounts after the stimulus are simulated. These time courses are then compared with experiment. The simulation is repeated, adjusting model parameters, until optimal agreement is obtained between simulated and experimental data. For some parameters, such as Michaelis constants, *in vitro* estimates may exist. In this case, the *in vivo* value is usually kept close to the *in vitro* value, unless this assumption makes it impossible to simulate experimental data.

The adjustment of parameter values is commonly done by trial-and-error; however, it is often preferable to use a computer program that repeats the simulation with many different sets of parameter values. In this case, after each repetition, a measure of the "distance" between the simulated and experimental time courses is computed. A commonly used measure sums the squares of the differences between simulated and experimental metabolite concentrations. The sum is taken over all concentrations and also over all experimental time points. Some type of optimization routine (Press, 1994) is commonly included in such computer programs to adjust parameters in a direction suggested by the "distance" calculations for the previous few simulations. The goal is to find parameter values that minimize the distance measure.

Parameter adjustment continues until one or more value sets are found for which the shapes and amplitudes of the simulated metabolite time courses approximate the experimental time courses. If this approximation proves impossible, a new model based on new equations is needed. Following successful simulation, ***key control parameters*** can be defined as those parameters that are tightly constrained by the need to reproduce experimental data. Relatively small variations in these parameters cause significant changes in model behavior. Key control parameters are often candidate points for biological regulation of the signaling pathway. Experiments that determine values of these parameters constitute stringent tests that can falsify a model.

Separation of Fast and Slow Processes to Simplify Models

Experimental data generally determine the time scale of interest for a model. For example, experimental data concerning gene expression have a time scale of minutes or hours, whereas data concerning enzyme reaction rates may have a time scale of seconds or minutes. Models that simulate experimental data with a long time scale can be simplified, and the number of differential equations reduced, when processes or reactions with a fast time scale are assumed to be at equilibrium. Conversely, to simulate data with a fast time scale, the dynamics of slow processes can be neglected. A variable associated with a slow process, such as the concentration of a gene product, should simply be treated as a parameter. This separation into fast and slow time scales, and correspondingly fast and slow variables, is widely used for simplification of models. Chapter 7 has illustrated such a separation in a model of neuronal electrical activity. In that model, $[Ca^{2+}]$ was the slow variable, and the fast variables were membrane potential and a channel gating variable w (see Figs. 7.21 and 7.22).

As another example, if Ca^{2+} dynamics are being modeled, the number of differential equations can sometimes be reduced by assuming the rapid binding of Ca^{2+} to a buffer is always at equilibrium (see discussion of Eq. 8). Another example underlies the derivation of the standard Michaelis–Menten equation. Recall that the underlying reactions assumed in this derivation are

$$\mathrm{E} + \mathrm{S} \xrightarrow{k_1} \mathrm{ES}, \quad \mathrm{ES} \xrightarrow{k_1} \mathrm{E} + \mathrm{S}, \quad \mathrm{ES} \xrightarrow{k_2} \mathrm{E} + \mathrm{P}.$$

Here, S is substrate, E is enzyme, and P is product. *In vitro* (although often not *in vivo*) the total concentration of enzyme, $E_{\mathrm{tot}} = [\mathrm{E}] + [\mathrm{ES}]$, is usually much less than the concentration of substrate, [S]. In this case, relaxation of [ES]to a quasi-steady-state value usually occurs on a fast time scale. By comparison, [S] and [P] change very slowly. It follows that [ES] will always be very near its quasi-steady-state value. Therefore, [S] and [P] can be thought of as fixed parameters that determine what value [ES] has at any time. A separate differential equation for [ES] is therefore not necessary. One simply fixes [P] and [S] in the reaction scheme above and obtains the steady-state value for [ES]. To obtain [ES] the rates of ES dissociation and formation are set equal:

$$(k_{-1} + k_2)[\mathrm{ES}] = k_1\,[\mathrm{E}][\mathrm{S}].$$

Then, one solves for [ES] and uses the conservation condition, $E_{\mathrm{tot}} = [\mathrm{E}] + [\mathrm{ES}]$, to eliminate [E]:

$$[\mathrm{ES}] = \left(\frac{k_1}{k_{\pm 1} + k_2}\right)[\mathrm{E}][\mathrm{S}] \left(\frac{k_1}{k_{\pm 1} + k_2}\right)(E_{\mathrm{tot}} \pm [\mathrm{ES}])[\mathrm{S}].$$

Another rearrangement gives an expression for [ES] in terms of [S]:

AU: OK? last numbered eg was 19b

$$[\mathrm{ES}] = \frac{E_{\mathrm{tot}}[\mathrm{S}]}{K_{\mathrm{m}} + [\mathrm{S}]}, \quad with\ K_m = \left(\frac{k_{\pm 1} + k_2}{k_1}\right). \qquad (20)$$

This "steady-state approximation" allows the dynamics of the slow variables [S] and [P] to be described by a single differential equation:

$$\frac{d[P]}{dt} = \pm\frac{d[\mathrm{S}]}{dt} = k_2[\mathrm{ES}] = \frac{V_{\max}[\mathrm{S}]}{K_{\mathrm{m}} + [\mathrm{S}]}, \quad \text{with } K_m \text{ as above and } V_{max.} = k_2 E_{\mathrm{tot}} \qquad (21)$$

This is the standard Michaelis–Menten equation. In contrast, two differential equations are needed when the steady-state approximation is not used. One equation describes the rate of change of [P] and the other is for the rate of change of [ES].

The general method for model simplification is as follows. First, the equilibrium values of the "fast" variables ([ES] in the above example) are solved for as a function of the "slow" variables ([S] in the above example). The slow variables are treated as parameters in this calculation. Then, one changes perspective, using the equilibrium values of the fast variables in the differential equations for the slow variables. Since these equilibrium values are now functions of the slow variables, the fast variables, and their differential equations, are eliminated from the model. Only the differential equations for the slow variables are left. These differential equations together are termed the "slow subsystem."

A second simplified model also results from this method. This model consists of the differential equations for the fast variables alone, with the slow variables represented by parameters. As was mentioned in Chapter 7, these differential equations constitute the "fast subsystem." When the method is applied to the original Hodgkin–Huxley model with four differential equations (Hodgkin and Huxley, 1952), the two simplified models consist of two differential equations each. The qualitative behavior of the simplified models can be analyzed and represented in an intuitively appealing manner, similar to that in Chapter 7 (Figs. 7.21 and 7.22) [see also Rinzel (1985)]. For further examples and for discussion of simplification by separation of spatial scales as well as time scales, see Ermentrout (2001).

SPECIFIC MODELING METHODS

Models Help to Analyze Metabolic Flux Regulation

One important goal of modeling biochemical pathways is to determine the parameters, such as amounts of particular enzymes, that control the rate at which substance flows from initial substrate to final product. An example would be the rate at which glucose is converted to pyruvate in glycolysis. This rate is termed the *metabolic flux* through the pathway. ***Flux regulation*** is necessary to keep metabolite concentrations within ranges appropriate to the state of the cell. Flux regulation of pathways such as glycolysis is also essential for balancing the production and use of ATP. Parameters to which metabolic fluxes are most sensitive are candidates for biological flux regulation.

The method of ***metabolic control analysis*** (MCA, also termed metabolic control theory) provides flux control coefficients to describe the importance of each enzyme in regulating the flux of metabolite through the pathway. These flux control coefficients provide a clear and concise representation of pathway regulation. The methodology of MCA is therefore briefly discussed. For a fuller treatment, Stephanopoulos *et al.* (1998) should be consulted. Limitations of MCA are as follows. The control coefficients are defined using the response of the pathway to small changes in enzyme activities. Large changes, such as may be caused by mutations in genes coding for enzymes, are not well handled. Also, MCA usually considers enzymes and metabolites to be at uniform concentrations throughout the cytoplasm.

In MCA, the sensitivities of the metabolic flux to changes in the activities of enzymes are expressed as ***flux control coefficients*** **(FCCs)**. With the steady-state metabolic flux through a pathway denoted by J and the activity of the ith enzyme in the pathway denoted by E_i, an FCC, F^i, is defined as follows. An infinitesimal change in E_i, dE_i, yields an infinitesimal change in J, dJ. The *relative*, or *fractional*, change in J is then defined as dJ/J. This relative change is divided by the *relative* change in E_i:

$$F^i = \frac{dJ/J}{dE_i/E_i} = \frac{d\ln J}{d\ln E_i}. \tag{22}$$

To understand FCCs, it helps to examine the relationship between pathway flux and enzyme activity. Figure 14.7 illustrates that the flux J will saturate as

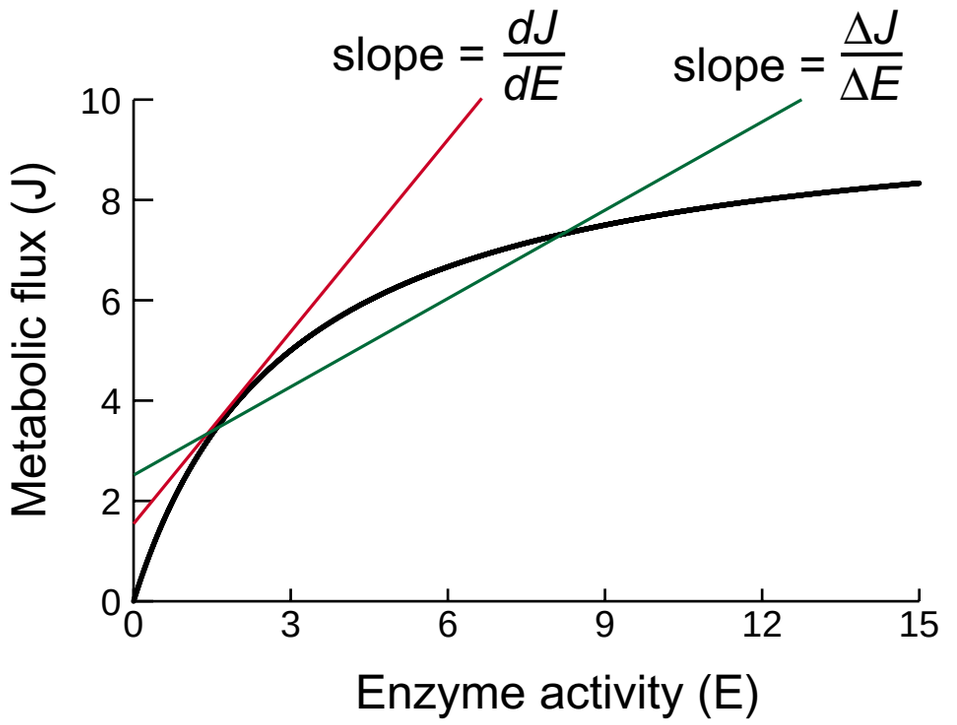

FIGURE 14.7 Metabolic flux versus activity of an arbitrary enzyme in a biochemical pathway. The flux saturates at a finite level as the enzyme activity is increased. An approximation of the rate of change of flux with enzyme activity is shown (slope of green line). This approximation is calculated using a large change ΔE in activity. For some values of E, the approximate rate of change can differ considerably from the true rate of change. This rate (slope of red line) is calculated using an infinitesimal activity change dE.

the activity or concentration of any given enzyme is increased. The slope of the graph of J versus enzyme activity is related to the FCC. To obtain the FCC, the slope of the tangent line (the derivative dJ/dE_i) is multiplied by the enzyme activity and then divided by J. Figure 14.7 also illustrates why infinitesimal changes in the enzyme activity are used to define FCCs. For a large change in enzyme activity, the inferred slope of the flux-versus-activity relationship (the fraction $\Delta J/\Delta E_i$) can be considerably different than the actual slope (the derivative dJ/dE_i). Therefore, FCCs inferred from systems with large changes in enzyme activities can differ considerably from actual FCCs. An extension of MCA has been developed to approximate FCCs from responses to large changes (Small and Kacser, 1993).

A ***summation theorem*** states that all the FCCs—one for each enzyme in the pathway—must add up to 1. A consequence is that most FCCs in long pathways must be small, so that the sensitivity of pathway flux to alterations in the activity of any one enzyme is usually low. By contrast, in short pathways several FCCs are often large, and the corresponding enzymes exert strong flux control.

One result of MCA has been to modify or overturn concepts of metabolic control that were guessed via intuition. For example, consider enzymes that are subject to feedback inhibition by their reaction products. These enzymes serve as control points of the metabolic flux through the pathway, because the feedback prevents the concentrations of their reaction products and of pathway end products from rising too high. Intuitively, one might expect that these enzymes are strongly rate-limiting, in the sense that small changes in their activity would have large effects on the pathway flux. However, MCA has demonstrated that this expectation is usually false (Stephanopoulos *et al.*, 1998). Instead, enzymes whose activities are affected by allosteric interactions with their substrates or products tend to have low FCCs.

Some applications of MCA have helped increase understanding of neuronal metabolism. For example, in several regions of rat brain, the flux control coefficient of the enzyme nitric oxide synthase (NOS) for the *in vivo* synthesis of nitric oxide (NO) has been determined (Salter, 1996). Administering varying dosages of an NOS inhibitor and measuring effects on the NO synthesis rate determined the FCC of NOS. In all regions, this FCC was found to be close to 1. Because the sum of all FCCs in a biochemical pathway must equal 1 by the summation theorem, other processes essential for NO synthesis must have low FCCs, and NOS must be rate-limiting for NO production. Other processes, such as the transport of the NO precursor L-arginine from blood into neurons, must also not be rate-limiting for NO production. In other biochemical pathways, this method could be used to quantify the flux control of any enzyme for which a specific inhibitor is available.

If a detailed kinetic model can be constructed for a biochemical pathway, with differential equations such as Eq. 11 that describe changes in the levels of each substrate and product, then regulation of pathway flux can be assessed without MCA. However, because MCA flux control coefficients provide a concise representation of pathway regulation, their prediction may still be valuable. Such predictions might be compared with experimental values to test the model's validity. Also, biochemical data may not suffice to estimate many parameter values in a detailed model. It may then be better not to present such a model, because unjustified detail can obscure the state of knowledge of pathway regulation. It would be preferable to experimentally determine flux control coefficients to concisely characterize pathway regulation.

MCA has recently been extended to begin considering concentration gradients within cells. FCCs have quantified the control exerted by macromolecule diffusion coefficients on the flux through a simple model biochemical pathway (Kholodenko *et al.*, 2000); however, a problem is that no experimental method has been devised to estimate diffusion FCCs.

Special Modeling Techniques Are Required if Enzymes Are Organized in Macromolecular Complexes

To maximize the efficiency and specificity of reactions, many biochemical pathways are organized so that successive enzymes are positioned close to each other. This organization is mediated by ***multienzyme complexes*** or ***signaling complexes***. These complexes are aggregates of macromolecules that contain groups of enzymes in combination with organizing "anchoring" proteins. Other proteins involved in signal transduction may be present, such as receptors for neurotransmitters or hormones. Further organization can be achieved by binding of the anchoring proteins to cytoskeletal elements. These signaling complexes are often based on reversible protein–protein binding reactions (Teruel and Meyer, 2000) so that an individual complex may not be very long-lived. However, the lifetimes of such complexes are likely to be long compared with the time scale of enzyme reactions and of intracellular transport of metabolites.

Several instances of such organization are now known. A complex of glycolytic enzymes can be organized by binding to actin filaments (Fokina *et al.*, 1997; Kurganov, 1986). In neurons, signaling pathways

using isoforms of MAPK appear to be organized into complexes. For example, scaffold proteins termed JIP proteins bind to particular isoforms of MAPK and MAPKK (Davis, 2000) and interact with kinases that activate MAPKK. As another example, PKA, calcineurin, and protein kinase C (PKC) bind to A-kinase anchoring proteins (AKAPS), which, in turn, bind cytoskeletal elements (Edwards and Scott, 2000). Finally, the NMDA receptor is in a large complex with more than 50 signaling proteins, kinases, and phosphatases (Husi *et al.*, 2000).

Two advantages of organizing signaling proteins into complexes are: (1) to favor a rapid passage of signals through an enzymatic cascade, and (2) to prevent unwanted cross-talk between signaling pathways. For example, if specific isoforms of MAPKK and MAPK are co-localized in complexes, then a given isoform of MAPKK will not be able to activate "improper" isoforms of MAPK. Also, a metabolite produced by an enzyme can be more efficiently passed on to the next enzyme in a pathway if both enzymes are co-localized.

Modeling signaling pathways organized into complexes may require equations specific to the system under study; however, some general comments can be made. Intermediate metabolites might not equilibrate with the cytoplasm *via* diffusion, but instead ***metabolic channeling*** may dominate. Metabolic channeling is defined as movement of a metabolite directly from one enzyme to the next within a multienzyme complex. In this situation, the rate of use of the intermediate metabolite by the next enzyme would not be a function of its bulk cytoplasmic concentration. Rather, it might be a direct function of the rate of production of the metabolite. If the metabolite was produced at a low rate, it might be immediately channeled to the next enzyme and used. If it was produced at a high rate, the channeling might saturate. Denoting the rate of metabolite production as $R_{\text{production}}$, this situation could be modeled with a Michaelis–Menten expression for the rate of usage of the metabolite, R_{usage}:

$$R_{\text{usage}} = \frac{V_{\max} R_{\text{production}}}{R_{\text{production}} + K_S}. \qquad (23)$$

AU: OK? last numbered eg was 22

Here, $V_{\max}$ and K_s correspond to the maximal velocity and Michaelis constant of the second enzyme in a standard Michaelis–Menten equation (Eq. 10). However, the units and therefore the numerical values of these parameters are different in Eq. 23 than in Eq. 10. Metabolic control analysis, discussed above, can be extended to assess flux regulation within a signaling pathway containing multienzyme complexes (Stephanopoulos *et al.*, 1998).

A recent model (Levchenko *et al.*, 2000) illustrates possible kinetic effects of a scaffold protein that is assumed to bind both MAPKK and MAPK in a complex, allowing interaction of the two enzymes. As shown in Fig. 14.8, this model assumes reversible binding of MAPKK and MAPK to the scaffold protein. Both MAPKK and MAPK must be doubly phosphorylated to be active. In solution, these phosphorylations occur sequentially. However, the model assumes that when either enzyme is bound to the scaffold protein, both phosphorylations occur simultaneously, hence the absence of singly phosphorylated MAPKK and MAPK in Fig. 14.8. Another assumption is that only inactive MAPK and MAPKK can bind to the scaffold. Thus, if MAPK or MAPKK is activated while bound to the scaffold, and then dissociates from the scaffold, it cannot rebind until the phosphates are removed. At present, neither of these assumptions has been confirmed experimentally.

Both of these assumptions are, however, necessary to support the results of simulations (Levchenko *et al.*, 2000) with the model of Fig. 14.8. One result is that the presence of scaffold protein reduces the steepness of the dose–response curve for MAPK activation as a function of stimulus strength, when stimulus strength is represented by the activity of MAPKKK. This result depends on the assumption that the dual phosphorylations of MAPKK or MAPK in the scaffold are simultaneous. A second result is that for fixed stimulus strength, as the concentration of scaffold protein is increased, the percentage of activated MAPK at first increases, but then decreases. The increase is due to the assumption of simultaneous dual phosphorylations when MAPKK and MAPK are bound to the scaffold, because simultaneous phosphorylations are more efficient than the sequential phosphorylations that occur in solution. The decrease in MAPK activation when the level of scaffold protein is made very high does not depend on the above assumptions. Rather, it comes about because complexes of scaffold protein with only one inactive enzyme (MAPKK or MAPK) account for an increasing proportion of total enzyme as scaffold concentration is increased.

Random Fluctuations in Molecule Numbers Influence the Dynamics of Biochemical Reactions

Rather than using chemical concentrations as variables, the stochastic level of modeling uses the actual numbers of each molecular species. In this way, one can include ***random variability*** in the times of synthesis and degradation of individual macromolecules or metabolites. For some macromolecules, such as

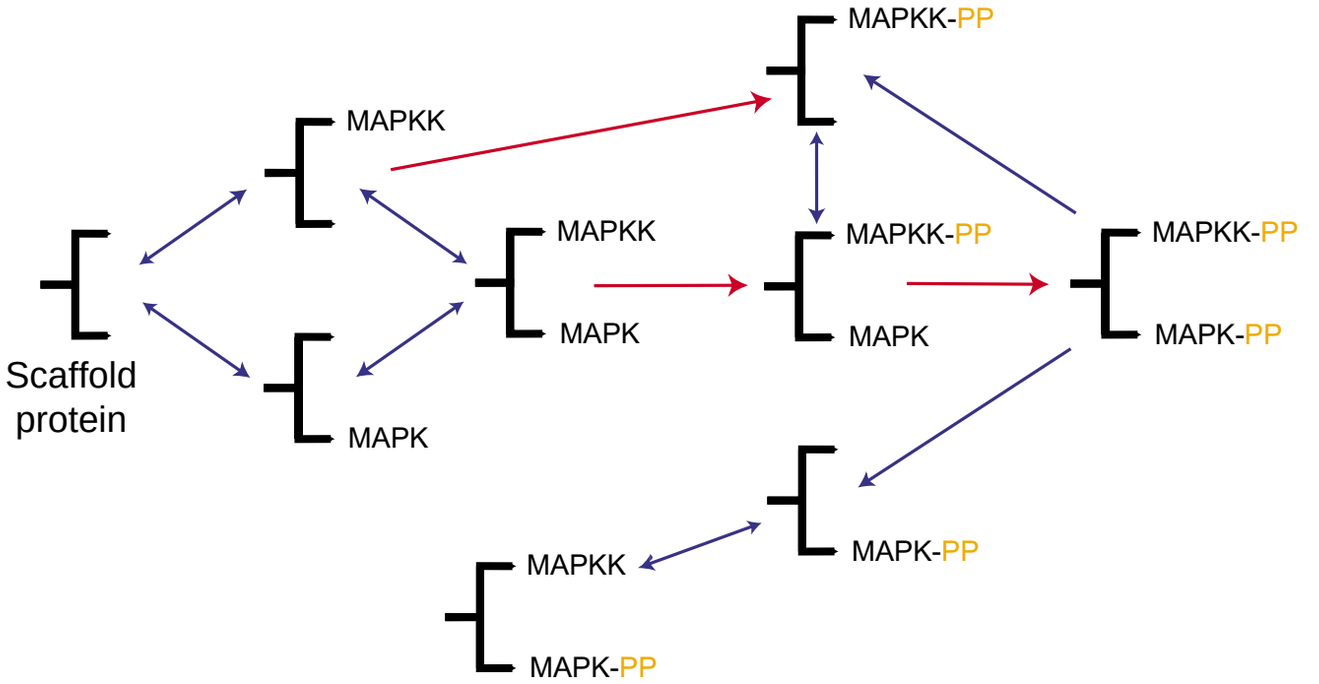

FIGURE 14.8 Model of a scaffold protein able to reversibly bind both MAPK and MAPKK. Nine biochemical species are possible: free scaffold, scaffold with unphosphorylated MAPK and/or MAPKK bound, and scaffold with doubly phosphorylated MAPK and/or MAPKK bound. Transitions between species can be due to kinase association or dissocation from the scaffold (blue arrows) or to phosphorylation of kinases (red arrows). Reverse transitions due to dephosphorylation are not modeled. Dissociation of phosphorylated kinases is irreversible (single-direction blue arrows). For clarity, only some possible dissociations are shown.

specific mRNAs and transcription factors, average molecule numbers per cell can be modest. They may be on the order of a hundred or less. In this case, variability in the times of single-molecule synthesis or degradation lead to significant ***stochastic fluctuations*** in macromolecule numbers (McAdams and Arkin, 1999). These fluctuations are seen as random variations about a mean number of molecules, and their presence can considerably alter the dynamics of biochemical pathways. For example, stochastic fluctuations of the numbers of enzymes or metabolites in signaling pathways might cause large variability in the response of individual members of a cell population to a stimulus (Levchenko *et al.*, 2000; McAdams and Arkin, 1998). Only a fraction of cells might give an observable response, such as differentiation following application of a hormone. A rule of thumb is, if there are fewer than ~200 to 300 copies of any important macromolecule or metabolite, stochastic fluctuations may significantly affect dynamics.

Stochastic modeling has recently yielded qualitative insights into how fluctuations are expected to affect the dynamics of a biochemical pathway. For example, fluctuations are expected to most commonly decrease the steepness of a nonlinear stimulus–response relationship, such as that in Fig. 14.4B for MAPK activation (Berg *et al.*, 2000). However, in specific circumstances the steepness can increase (Paulsson *et al.*, 2000). Also, via a phenomenon known as stochastic resonance, fluctuations can increase the reliability or magnitude of responses to small signals (Stacey and Durand, 2001). These results are qualitative, and the effects of fluctuations within specific signaling pathways in neurons have not been studied. This is because of the difficulty in estimating average values for the absolute numbers of important macromolecules per cell. Such estimates are very difficult for cells with a complex morphology, such as neurons. These estimates are, however, essential prerequisites to quantitative modeling of fluctuations. Currently, data sufficient to allow detailed stochastic modeling exist for only a few prokaryotic pathways (Arkin *et al.*, 1998).

To carry out computational simulations that include stochastic fluctuations, the equations of a biochemical model are first formulated according to the continuous, or differential-equation-based, approach. Concentrations are the variables. Differential equations such as Eqs. 11 and 14–17 determine how the variables evolve. Then, the variables are changed

from concentrations to molecule numbers. This requires rescaling parameters such as maximal enzyme velocities and Michaelis constants to reflect the change in units; however, the form of the differential equations remains unchanged. The deterministic rate of each individual reaction is still computed from these equations. For example, in Eq. 11, the first term on the right-hand side gives the rate of the reaction that synthesizes P from the substrates S_1 and S_2.

These reaction rates have units of molecules per second. The reciprocals of these rates give the average time intervals between successive occurrences of each specific reaction. For a given reaction, such a time interval is denoted by T_{avg}. For simulating fluctuations in molecule numbers, one can proceed as follows. The time step is chosen small enough (much less than all the T_{avg} values) so that the probability of each reaction occurring during a step is only a few percent. At each time step, a random number is chosen for each reaction. Each number is chosen from a uniform distribution on the interval {0,1}. Whether a specific reaction occurs during the time step can be determined by whether its random number is greater or less than the reaction probability. That probability is the product of the reaction rate and the time step. If a reaction occurs, the appropriate molecule numbers are changed by 1 or –1.

Another accurate and rapid algorithm (Gillespie, 1977) uses the following result from statistical physics. If a particular biochemical reaction occurs at a time t arbitrarily taken to be 0, the probability $P(t)$ that the *next* reaction of that type will occur within a small time interval Δt that is centered at $t > 0$ is

$$P(t) = \frac{\Delta t}{T_{avg}} \exp\left(\frac{\pm t}{T_{avg}}\right), \qquad (24)$$

with T_{avg} defined as in the last paragraph. For an implementation of Eq. 24 suited to systems with many molecular species, see Gibson and Bruck (2000).

Both of the above methods are limited in that only changes in the total number of molecules of each chemical species are simulated. Individual molecules are not represented. Thus, the fate of particular molecules cannot be traced, and therefore diffusion or spatial localization of molecules cannot be simulated. This limitation can be overcome by using an algorithm that represents each molecule as an individual object. At each time step this object is able to diffuse and also has probabilities of undergoing reactions. One software package that embodies this approach is StochSim, developed by Firth and Bray (2001) and colleagues. Such a package is particularly useful in simulating the dynamics of a signaling complex of associated proteins, containing enzymes and receptors specific to one or more intracellular signaling pathways. Conformational changes, covalent modifications, and ligand binding are assumed to switch the complex between a series of possible states, and the state trajectory can be followed (Morton-Firth *et al.*, 1999). Such simulations are needed to help understand how the NMDA receptor complex, or other neuronal complexes, transmits signals.

Consider a pathway for which a model based on continuous concentration variables predicts oscillations or multiple stable steady states of metabolite concentrations. Large fluctuations could disrupt the oscillations or destabilize the steady states (Barkai and Leibler, 2000; Smolen *et al.*, 1999). Therefore, predictions of behavior that neglect fluctuations may be false. Nevertheless, for many biochemical pathways, continuous models consisting of sets of differential equations (*e.g.*, Eqs. 14–17) remain essential because of insufficient data to justify a stochastic model. Generally, much of the data used to construct a continuous model consist of large and relatively reproducible changes in pathway fluxes and metabolite concentrations following strong stimuli. Because those responses are reproducible, a continuous model may be expected to reliably predict responses to new stimuli similar in strength to those used in model construction.

Genes Can Be Organized into Networks That Are Activated by Signaling Pathways

Gene regulation is a common endpoint of biochemical signaling pathways. As discussed in Chapter 13, signaling pathways often activate proteins termed transcription factors (TFs) (Karin, 1994). The activation is often via phosphorylation of critical amino acid residues. Activated TFs regulate the transcription of genes by binding to nearby short segments of DNA. In Chapter 13, these segments were referred to as *cis*-regulatory elements. Another common terminology is ***response elements***. If these elements activate transcription, they are commonly termed enhancers; if they repress transcription, they are commonly termed silencers. Many genes are regulated by multiple TFs. Genes coding for TFs can be repressed or activated by TFs, including their own products.

Large clusters of genes are often regulated in concert by biochemical signaling pathways that activate specific TFs. For example, activation of MAPK can lead to activation of hundreds of genes and repression of many others (Roberts *et al.*, 2000). ***Gene networks*** may be defined as gene clusters in which the expression of some members is regulated by the protein products of other members or by a common

input such as a neurotransmitter binding to a G protein–coupled receptor. Thus, the expression of network genes varies in a coordinated manner. Gene networks mediate long-term processes such as development and memory formation. Understanding these processes therefore requires an understanding of the dynamics of gene networks.

One gene network often implicated in the control of synaptic plasticity and memory formation is the network based on transcriptional regulation by the family of TFs that includes CREB (Mayford and Kandel, 1999; De Cesare and Sassone – Corsi, 2000; Lonze and Ginty, 2002; Bartsch *et al.*, 1998; Yin and Tully, 1986). Figure 14.9 illustrates aspects of this network, many of which are discussed in more detail in Chapter 13. Neurotransmitters, such as serotonin, bind to receptors and activate G proteins. Production of intracellular second messenger molecules, such as cAMP, is enhanced. Kinases, such as PKA and MAPK, are activated as a result. These kinases phosphorylate CREB and related TFs. A positive-feedback loop appears to exist in this network (Fig. 14.9). In this loop, phosphorylated CREB, when bound to CREs in the vicinity of the *creb* promoter, activates *creb* tran-

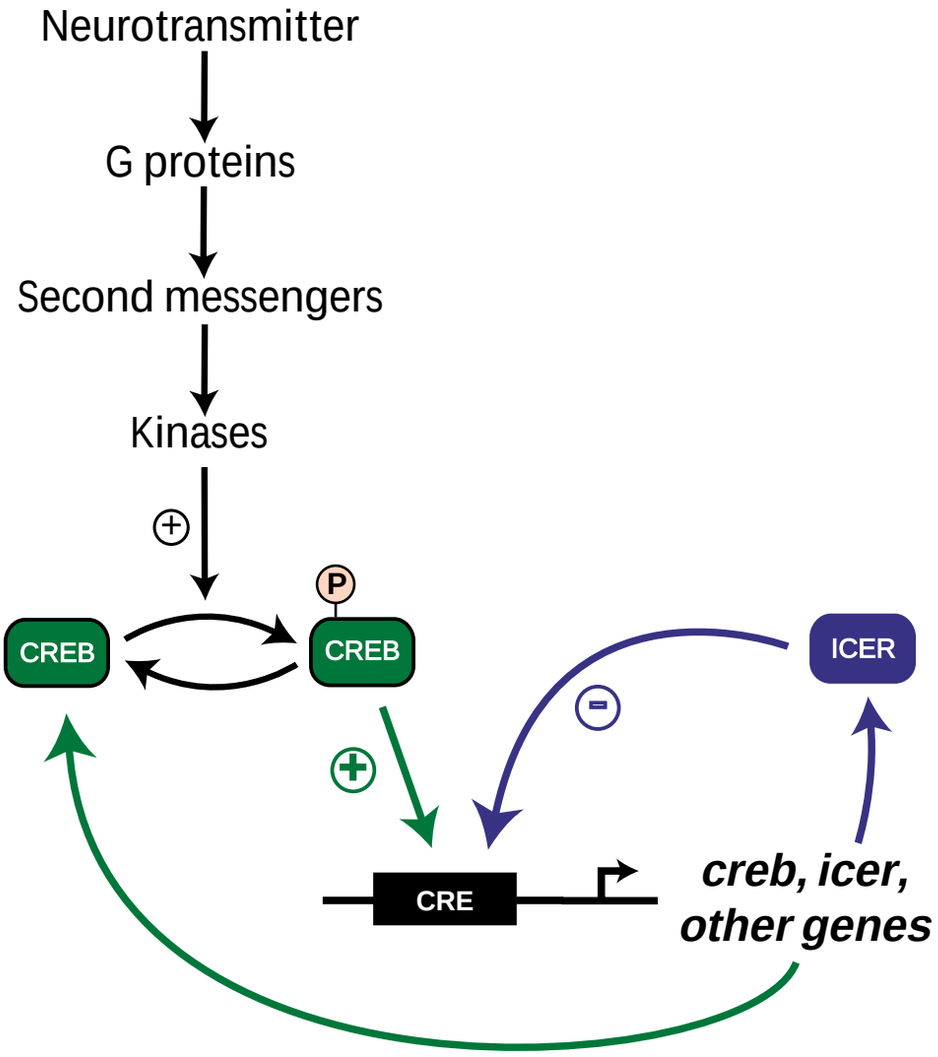

FIGURE 14.9 Signaling pathway involving transcriptional regulation by CREB. Neurotransmitters such as serotonin bind to receptors and act through G proteins to elevate levels of intracellular messengers (e.g., cAMP, Ca^{2+}). Kinases such as PKA are activated, resulting in phosphorylation of CREB and related TFs. Phosphorylated CREB stimulates the transcription of genes when bound to enhancer sequences termed Ca^{2+}/cAMP response elements (CREs). Possible feedback interactions among the genes coding for CREB and related TFs are shown. A positive-feedback loop (green arrows) may regulate CREB synthesis. In this loop, CREB binds to CREs near *creb* and activates *creb* transcription. The repressor ICER is an element of a negative-feedback loop (blue arrows). Transcription of *icer* is increased when the level of CREB increases, and ICER, in turn, can bind to CREs near the *creb* gene, repressing *creb* transcription.

scription (DeCesare and Sassone–Corsi, 2000; Walker *et al.*, 1995). There is also a negative-feedback loop. CREB induces the gene for another TF of the CREM/CREB family (Chapter 13) termed inducible Ca^{2+}/cAMP-responsive early repressor (ICER) (Molina *et al.*, 1993). ICER is a powerful transcriptional repressor. On binding to CREs, ICER represses *icer* transcription and also that of *creb*, closing the negative-feedback loop.

Experimental data essential for understanding the dynamics of gene networks are obtained by several methods. For example, sets of time courses of the mRNA levels expressed by large numbers of genes allow characterization of the response of cells or tissues to stimuli (Roberts *et al.*, 2000) or characterization of genetic disease states (Mirnics *et al.*, 2000). Current technology allows the expression time courses of ~10,000 genes to be simultaneously followed via quantification of their mRNAs. Cross-talk between signaling pathways can take the form of convergent activation of groups of genes by several pathways, and can be identified from mRNA time courses. Understanding neural plasticity requires determining expression time courses for genes involved in synaptic modification. Further complexity exists because protein levels are often not well correlated with mRNA levels. Therefore, time courses of protein levels also need to be characterized (Ryu and Nam, 2000).

Understanding genetic regulation requires more than collecting large numbers of mRNA and protein time courses. A framework is required for expressing the biochemical architecture of genetic systems and for extracting genetic regulatory relationships from large sets of gene expression data. The precision of mathematical language makes modeling the natural framework (Smolen *et al.*, 2000). Models are also important for predicting the response of gene networks to novel pharmacological or chemical agents.

AU: The sentence "The precision ... natural framework makes no sense? Pls clarify

Modeling studies of gene networks have often used qualitative models with modest numbers of equations and parameters. These models assess the behaviors of networks with common biochemical elements (Smolen *et al.*, 2000). Such elements include formation of TF dimers or oligomers, and positive- and negative-feedback loops in which TFs activate or repress transcription of their own or each other's genes. These models give insight into the behaviors more complex gene networks exhibit, and are used below to illustrate the dynamics generated by typical regulatory schemes. Relatively few models have considered regulation of mRNA processing or translation (Cao and Parker, 2001). Therefore, the discussion below focuses on transcriptional regulation.

First, mathematical analysis of gene expression data is briefly discussed. mRNAs are extracted at a series of time points following exposure to a hormone or other stimulus, and then hybridized to *DNA chips* to determine the relative amounts of mRNAs at these time points (Cerhold *et al.*, 1999; Wen *et al.*, 1998). A technique termed *cluster analysis* is applied to the time courses of the mRNAs (Ramoni *et al.*, 2002). This technique groups genes with expression time courses of similar shape. Such clusters may be regulated by a common factor, such as a specific TF. Methods are being developed to efficiently use clustered gene expression data to construct models of regulation within gene networks (Toh and Horimoto, 2002). Model parameter values are adjusted until the time courses for mRNA concentrations following a simulated stimulus approximate the experimental responses. A shortcoming of cluster analysis is that it assumes (1) gene network regulation is hierarchical, and (2) genes performing similar functions exhibit similar expression patterns. Methods that are not restricted by the above assumptions are being developed (Yeung *et al.*, 2002; Ihmels *et al.*, 2002).

Methods Exist to Model Gene Networks at Very Different Levels of Detail

The Logical-Network Method Regards Genes as Simple ON–OFF Switches

In the *boolean*, or *logical-network*, *method*, modeling is rather crude, but simulations can be carried out rapidly. The rate of transcription of each gene is assumed to be a boolean logical variable: either ON (a fixed transcription rate) or OFF. Control of gene expression is modeled by simple rules about which genes are activated or repressed by others. Relatively large time steps are taken in simulations. Figure 14.10 illustrates a simple model of this type.

In Fig. 14.10, three genes have their expression updated according to the following rules: (1) Gene 1 is ON only if Gene 2 was ON at the previous time step and gene 3 was OFF, (2) Gene 2 is only ON if Gene 1 was OFF at the previous time step, (3) Gene 3 is only ON if Gene 1 was ON at the previous time step. Figure 14.10A shows schematically these interactions between genes with plus (activating) signs and genes with minus (suppressing) signs. The behavior of this model is rather simple, as illustrated in Fig. 14.10B. Irrespective of the initial state of the genes, the model rapidly enters and remains in a specific oscillation in which four network states occur in a fixed, repeating order. Boolean models of gene networks can be

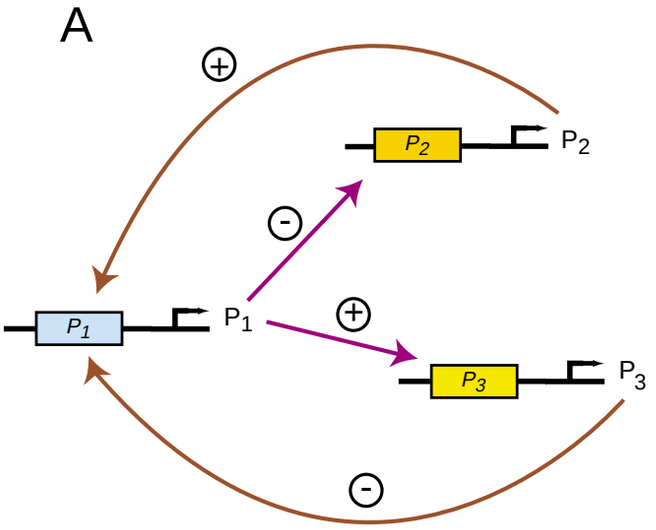

FIGURE 14.10 A simple logical-network gene model. (A) Interactions among three genes. The protein product of gene 1 represses transcription of gene 2 and activates transcription of gene 3, the product of gene 2 activates gene 1, and the product of gene 3 represses gene 1. (B) When these interactions are implemented as the logical rules described in the text, then during a simulation, the activity state of the three genes changes at each time step. However, irrespective of the initial state, the model quickly enters a repeating cycle of four network activity states (outlined by the dashed box).

efficiently constructed from large sets of gene expression data (Wen *et al.*, 1998; Toh and Horimoto, 2002). Because it models regulation so crudely, the logical-network method is suited only for large networks in which it is not feasible to study in detail the regulation of most of the genes.

The Continuous Method Is More Accurate but Computationally Intensive

With the continuous approach, differential equations are written to describe the rates of change of important mRNA and protein concentrations. These equations contain terms to represent processes such as macromolecular synthesis, degradation, and association of monomers into oligomers. Regulation of transcription is included in terms describing the synthesis of mRNA. As an example of a simple model that produces interesting behavior, consider the case of a single gene, *tf-a*, whose protein product is denoted TF–A. TF–A activates *tf-a* transcription, thereby forming a positive-feedback loop. It is assumed that two TF–A molecules must bind together, forming a dimer, which then binds to an enhancer sequence near the *tf-a* promoter (Fig. 14.11A). The corresponding differential equation for the rate of change of *tf-a* mRNA concentration is

$$\frac{d[tf \pm a\ \text{mRNA}]}{\text{dt}} = \frac{k_{\max}[\text{TF} \pm \text{A}]^2}{[\text{TF} \pm \text{A}]^2 + K_d} \pm k_{\text{degR}}[tf \pm a\ \text{mRNA}] + R_{\text{bas}}. \quad (25)$$

In Eq. 25, the first term on the right-hand side gives the transcription rate of *tf-a* as a saturable function of TF–A concentration. The second term accounts for first-order degradation of *tf-a* mRNA. The third term accounts for a low rate of transcription, R_{bas}, in the absence of activation of the *tf-a* gene by TF–A. At high [TF–A] the transcription rate approaches a maximal value $k_{\max}$. TF–A dimers regulate transcription, and in Eq. 25, the square of TF–A concentration is used to crudely approximate the concentration of TF–A dimers. The justification for this is as follows. From elementary kinetics, the rate of formation of TF–A dimers is proportional to the square of TF–A monomer concentration, and can be written as k_{f} [TF – A]$_{\text{mon}}$ [TF – A]$_{\text{mon}}$. The dissociation rate of dimers is proportional to dimer concentration, and can be written as k_{b} [TF – A]$_{\text{dim}}$. As discussed previously (following Eq. 6), a rapid-equilibrium approximation can be made by setting the association and dissociation rates equal to each other. Then, solving for dimer concentration yields a proportionality to the square of monomer concentration

$$[\text{TF} \pm \text{A}]_{\text{dim}} = {}^{k_{\text{f}}}\!/_{k_{\text{b}}}\,[\text{TF} \pm \text{A}]_{\text{mon}}[\text{TF} \pm \text{A}]_{\text{mon}}. \quad (26)$$

If most TF–A is monomeric, then Eq. 26 implies that [TF–A]$_{\text{dim}}$ is approximately proportional to the square

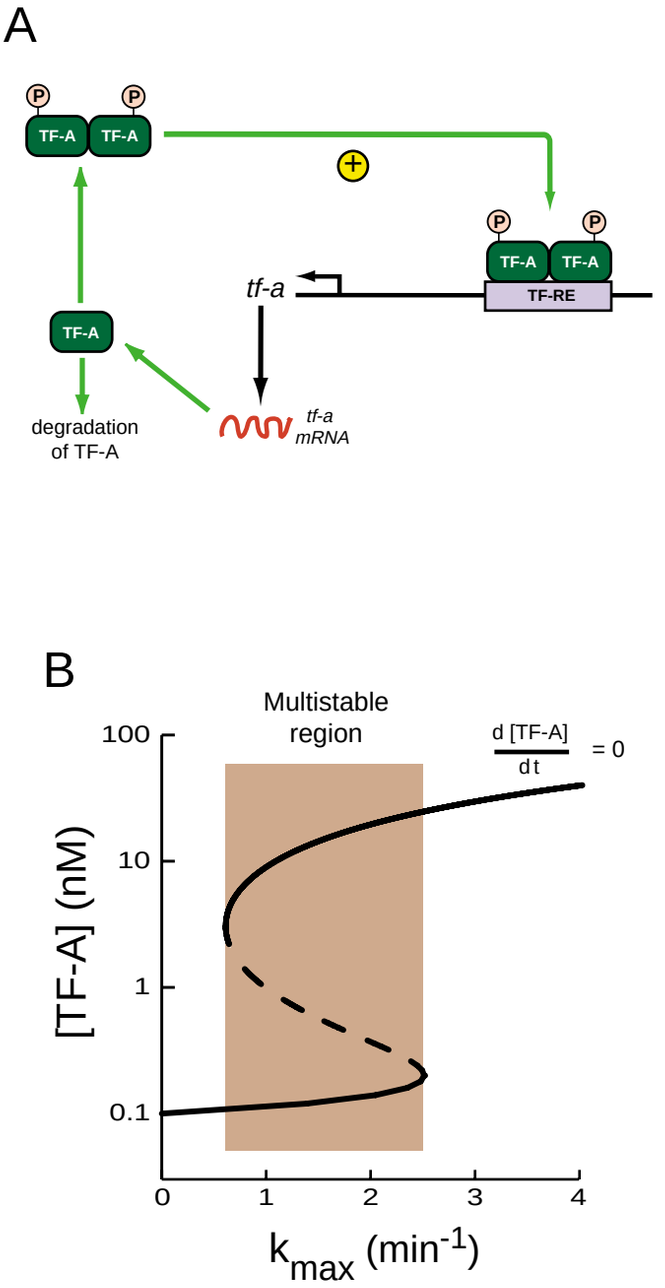

FIGURE 14.11 Positive autoregulation of a single gene. (A) Schematic of the model. Phosphorylated dimers of TF–A activate *tf-a* transcription when bound to a response element, termed a TF-RE, near the TF–A promoter. Degradation of TF–A protein is also indicated. (B) Bistability in the model of (A). For 0.6 min^{-1} < $k_{\max}$ < 2.5 min^{-1} (brown region in figure) two stable steady-state solutions of [TF–A] exist (lower and upper portions of the steady-state curve along which $d[\text{TF–A}]/dt = 0$). There is an unstable steady solution between (dashed). Outside the brown region there is only a single stable solution.

of total [TF–A], which is the assumption of Eq. 25.

Along with Eq. 25, a second differential equation is needed for TF–A protein concentration. If TF–A protein was immediately translated from mRNA, a simple equation might be assumed, with two linear terms for TF–A synthesis and degradation:

$$\frac{d[\text{TF} \pm \text{A}]}{dt} = k_{2,\text{f}}\left[tf \pm a\ \text{mRNA}\right] \pm k_{2,\text{d}}[\text{TF} \pm \text{A}]. \quad (27a)$$

If one wishes to take into account the time delay required for mRNA processing and transport, Eq. 27a can be modified to a *delay differential equation*:

$$\frac{d[\text{TF} \pm \text{A}]}{dt} = k_{2,\text{f}}\left[tf \pm a\ \text{mRNA}\right](t \pm \tau) \pm k_{2,\text{d}}[\text{TF} \pm \text{A}]. \quad (27b)$$

Here, the quantity (t-τ) in the first term on the right-hand side indicates that the concentration of *tf–a* mRNA at a given time is used to determine the rate of appearance of TF–A protein at a time τ min later. Delay differential equations are commonly used to represent slow kinetic processes. These equations exhibit a rich variety of dynamic behaviors (MacDonald, 1989).

The relatively simple model of Eqs. 25–27 can generate complex behavior (Smolen *et al.*, 1998, 1999). Figure 14.11B is a bifurcation diagram displaying the ways in which the dynamics of [TF–A] change as the parameter $k_{\max}$ is varied. With appropriate parameter values, the model is bistable. The curve traces the stable solutions of [TF–A] and of the *tf–a* transcription rate. Along this curve, the derivatives in Eqs. 25, 27a, and 27b are zero. At low values of $k_{\max}$ there is only one stable solution. Stimulus-induced phosphorylation of TF–A could make TF–A more effective at activating transcription, thereby increasing $k_{\max}$. When $k_{\max}$ is raised into the brown region in Fig. 14.11B two stable steady states exist (lower and upper portions of curve) with an unstable solution between (middle, dashed portion of curve). For even higher values of $k_{\max}$ there is again a single stable solution.

The following discussion may help to further understand the two steady states. In the lower state, there is virtually no activation of the positive-feedback loop in which *tf–a* activates its own transcription, because [TF–A] is very low. A small degradation rate, proportional to [TF–A], is balanced by a small basal rate of *tf–a* transcription. If [TF–A] is increased, positive feedback occurs, and TF–A dimers activate *tf–a* transcription in a regenerative process. The rate of transcription and TF–A protein synthesis is then faster the rate of than TF–A degradation. At a high concentration of TF–A protein, the positive feedback

saturates as the TF–RE enhancer becomes fully occupied with TF–A dimers. A maximal transcription rate is approached. But the TF–A degradation rate still increases with [TF–A] because it is directly proportional to [TF–A] in Eqs. 27a and 27b. Therefore, at a sufficiently high value of [TF–A], the degradation rate of TF–A must "catch up" with the synthesis rate. The second steady state is thereby created. If the model is initially at either stable solution, it will return to that solution after a small induced change in [TF–A]. However, a large induced change in [TF–A] can switch the system between steady states. An example might be a stimulus-induced phosphorylation of TF–A that causes a large but temporary change in k_{max}. In this case, after k_{max} returns to its original value, the concentration of TF–A will remain at the new value.

In comparing methods of modeling gene networks, the continuous method using differential equations is often preferred over the boolean method (model of Fig. 14.10). Greater physical accuracy is inherent in the use of continuous, rather than ON–OFF, gene expression rates. Furthermore, simulations using the boolean approach can erroneously predict behavior. Oscillations in gene expression seen with a boolean model may disappear when a more accurate, differential equation-based model is used (Bagley and Glass, 1996). Steady states may also disappear (Glass and Kauffman, 1973). Finally, methods of *bifurcation analysis* (Frank, 1978; Wiggins, 1990) can be applied to models based on differential equations. As discussed in Chapter 7, bifurcation analysis allows visualization of how the behavior of a model varies as a function of parameter values.

The continuous method, however, is more computationally intensive than the boolean method, because the former method requires much smaller time steps in simulations. For this reason, and because of the impracticality of thoroughly characterizing the expression kinetics of many genes, the boolean method is sometimes regarded as reasonable for large gene networks.

In both the boolean and continuous methods, intracellular transport of mRNA or protein can be modeled only in an *ad hoc* fashion. Time delays can be used, as in Eq. 27b, to represent the time between synthesis of a macromolecule in one intracellular compartment and its arrival and function in another compartment. For active transport of macromolecules, this is a reasonable approach (Smolen *et al.*, 1999). For diffusive transport, more accurate modeling would require discretizing the intracellular space into small volume elements, as was discussed for Ca^{2+} diffusion earlier in this chapter. It may be important to model transport, particularly in extended cells such as neurons. In neurons, delays of hours can be associated with transport of protein or mRNA from the soma to synapses targeted for long-term modification.

Simulations of macromolecular transport coupled with gene expression dynamics in neurons have not yet been reported. However, simulations of gene regulation in cells with simple shapes, such as a spherical nucleus in a spherical cell, have been carried out. These studies have found large differences in gene expression dynamics depending on whether transport of mRNA and protein from nucleus to cytoplasm and vice versa is assumed to be primarily active or primarily diffusive (Smolen *et al.*, 1999; Busenberg and Mahaffy, 1985). If active transport is modeled by a fixed time delay required for transit (Eq. 27b), then longer transit times tend to destabilize steady states of gene expression rates and favor oscillations. By contrast, in diffusion-dominated systems, slow diffusion tends to damp oscillations and yield steady states. These results suggest that dynamics of neuronal gene expression and synaptic modification may depend critically on the mode of macromolecular transport.

Gene Network Models Suggest That Feedback Loops and Protein Dimerization Can Generate Complex Dynamics

Transcription factors commonly bind to their target sequences as dimers. Dimerization of TFs steepens the relationship between the level of TF and the strength of the regulatory effect. Steepening this relationships favors complex dynamics, such as multiple stable gene expression rates and oscillations in gene expression rates. Complex dynamics are also favored if the regulated gene lies within a positive- or negative-feedback loop in which a gene activates or represses own expression. In Keller (1995), four models are described that include feedback loops and dimerization of TFs. These models exhibit multiple stable gene expression rates. In each model, if dimerization of TFs does not occur, only a single steady state is obtained. However, dimerization of TFs is not an absolute requirement for multistability. Keller (1995) also gives conditions for multistability in two models with monomers. In one model, two TFs each repress the other's transcription, and in the second, a TF activates its transcription by binding to multiple enhancers.

Positive Feedback in Gene Networks Favors Multistability, and Negative Feedback Favors Oscillations

Positive feedback is usually essential for multistability of gene expression rates (Thomas *et al.*, 1995).

For example, both positive feedback and TF oligomerization are essential for bistability in a model of neural tissue development in the *Drosophila* embryo (Kerszberg and Changeux, 1998). This model simulates the development of a group of undifferentiated cells into a structure of neurons that resembles an embryonic neural tube. Bistability in gene expression rates is essential for simulating the development of well-defined, smooth boundaries between neural and nonneural cells. In the simulation proneural genes are ON within a spatially restricted region and OFF outside that region.

A key element of this model is a switch in which bistability of gene expression rates is created by competition between homodimers of two TFs. Each TF homodimer activates expression of its own gene while repressing the gene for the other TF. Figure 14.12 illustrates this competition. This scheme constitutes a positive-feedback loop. An increase in the level of one TF, by repressing the formation of the second TF, favors a further increase in the first TF. In each stable solution, the gene for one TF is strongly activated by its own product, which simultaneously represses the gene for the other TF. If TF-1 levels are high in a specific cell, that cell will differentiate into a neuron. If TF-2 levels are high, then TF-1 expression is repressed, and the cell will not become a neuron. Specific *Drosophila* TFs were suggested (Kerszberg and Changeux, 1998). TF-1 might correspond to the Asc gene product, and TF-2 to the E(spl) gene product.

In the complete model, protein–protein interactions between receptors on the membranes of adjacent cells were also included so that the development of each cell would be influenced by the state of neighboring cells. For each cell, the state of the neighboring cells influences the transcription of the TFs in Fig. 14.12.

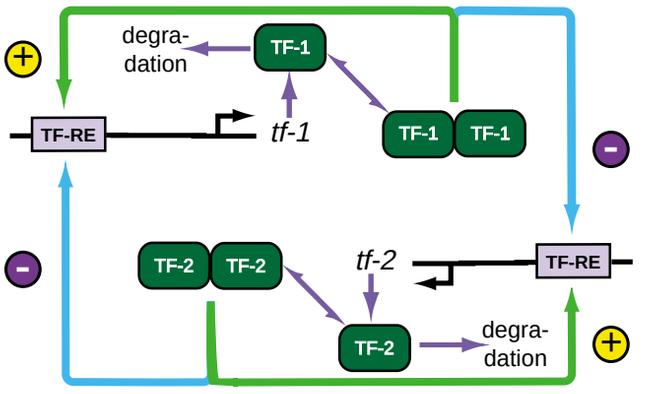

FIGURE 14.12 A simple gene regulatory scheme that generates bistability. The transcription factor TF–A activates expression of its own gene and represses the TF–B gene, whereas TF–B activates its own gene and represses the TF–A gene. Both TFs compete as homodimers for binding to response elements.

Therefore, for each cell, the choice of whether to differentiate into a neuron (corresponding to a state with TF-1 expression high and TF-2 expression repressed) or not (corresponding to TF-2 expression high and TF-1 expression repressed) depends on the state of the neighboring cell. These interactions between cells are critical for the development of boundaries between regions of neural and nonneural tissue (Kerszberg and Changeux, 1998).

Multistability in gene networks might be important in several biological processes. Steady states of gene expression rates could constitute information that could be preserved through cycles of cell division (Keller, 1994). Multistability in gene networks may be essential for cell differentiation (Thomas *et al.*, 1995; Laurent and Kellershohn, 1999). Because multistability is a manifestation of a positive-feedback loop, it has been suggested that genes involved in such loops are good candidates to regulate differentiation (Thomas *et al.*, 1995). However, none of these proposed roles for multistability have been experimentally verified.

Positive feedback alone usually cannot generate oscillations of rates of gene expression and therefore of macromolecule concentrations. In model gene networks, negative feedback is generally necessary to sustain oscillations (Smolen *et al.*, 2000). Many models describing oscillations also rely on dimerization of TFs (Goldbeter, 1996; Smolen *et al.*, 1998; Keller, 1995). A relatively simple model with negative feedback can be constructed by adding a second TF to the model of Fig. 14.11A. As diagrammed in Fig. 14.13A, this second TF, termed TF-R, represses transcription of both its own gene and that for the transcriptional activator, TF–A. In turn, TF–A activates the transcription of both *tf-a* and *tf-r*. The differential equations corresponding to this model consist of (1) Eqs. 25 and 27 modified to include repression of *tf-a* transcription by TF-R, and (2) two additional differential equations that describe the rates of change of [*tf-r* mRNA] and [TF-R] (Smolen *et al.*, 1999). The modified version of Eq. 25 is

$$\frac{d[tf \pm a\ \text{mRNA}]}{dt} = \left(\frac{k_{\max}[\text{TF} \pm \text{A}]^2}{[\text{TF} \pm \text{A}]^2 + K_{\text{d}}}\right)\left(\frac{k_{\text{R}}}{[\text{TF} \pm \text{R}]^2 + K_{\text{R}}}\right) \pm K_{\text{degR}}[tf \pm a\ \text{mRNA}] + R_{\text{bas}} \qquad (28)$$

The model of Fig. 14.13A can readily generate stable oscillations in the concentrations of both mRNA and protein species (Fig. 14.13B). An important synergistic application of modeling and experiment is construction of simple genetic systems that generate bistability or oscillations, combined with modeling based on equations similar to Eqs. 25–28. In

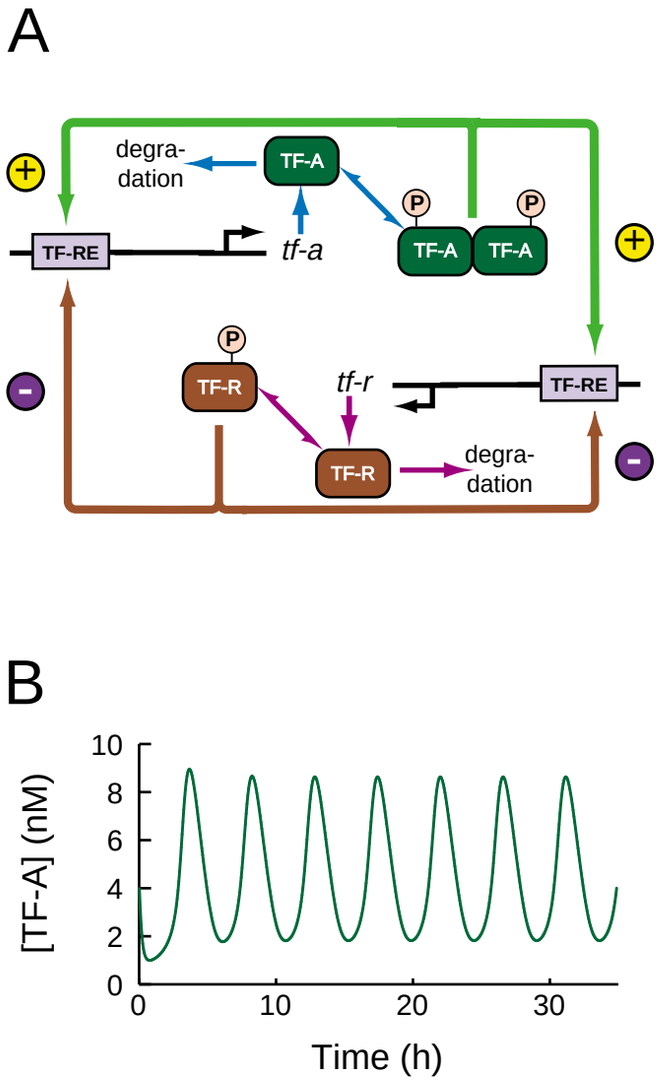

FIGURE 14.13 A simple two-gene network that sustaines oscillations. (A) Schematic of the model. A second transcription factor, TF–R, is added to the model of Fig. 14.11A. TF–A activates transcription by binding to TF–RE response elements, which are present near the promoter regions of both *tf-a* and *tf-r*. TF-R represses transcription by competing with the TF–A dimer for binding to both TF–REs. (B) Sustained oscillations of [TF–A] and [TF–R]produced by the model of (A).

one recent example (Gardner *et al.*, 2000) a bistable switch was constructed based on repression by two genes of each other's transcription. Modeling predicted perturbations that would flip the switch between states. In a second example (Elowitz and Leibler, 2000) a network of three genes was constructed. Gene 1 repressed gene 2, which repressed gene 3, which in turn repressed gene 1. This network constitutes a negative-feedback loop because expression of gene 1 ultimately leads to repression of gene 1. This system generated oscillations in transcription rates. Modeling predicted environmental conditions capable of sustaining oscillations.

Simple, designed genetic systems similar to the bistable switch or the three-gene network might prove useful for gene therapy. For example, transfection with several genes might confer novel drug responsiveness on target cells. Correction of a polygenetic disorder, in which several genes contribute to the observed phenotype, might also require transfection with multiple genes. Several promising methods for gene delivery to the brain are being developed, including viral transfection and cerebral injection of neural stem cells (Hsich *et al.*, 2002). Models are likely to be essential for predicting and understanding the responses of multiple transfected genes, or even a single gene, *in vivo*. Models have already helped to design gene vectors with maximal transfection efficiency (Varga *et al.*, 2001).

The positive- and negative-feedback loops within the gene network involving CREB and related TFs (Fig. 14.9) might support complex dynamics such as oscillations in transcription rates. Oscillations of CREB mRNA have been studied in endocrine cells (Walker *et al.*, 1995), and these feedback loops were suggested to be responsible.

Negative Feedback Underlies Circadian Rhythm Generation

A group of gene networks in which negative feedback appears essential for oscillations in gene expression is responsible for ***circadian rhythms***, which have evolved in most organisms exposed to daylight (Gartner, 1990; Dunlap *et al.*, 1999; Reppert and Weaver, 2001). These behavioral rhythms are self-sustaining in constant darkness. In circadian oscillators that have been well characterized, the products of one or a few core genes repress their own transcription in a cyclic fashion. Following the onset of repression, there is a delay of several hours, after which the repressing proteins are degraded, relieving repression (Dunlap *et al.*, 1999). For example, in *Drosophila* neurons that drive the circadian behavior rhythm, a transcription factor termed PER represses transcription of its own gene. Over many hours, PER becomes multiply phosphorylated and then degrades. Degradation relieves autorepression of *per* by PER, and another surge of transcription initiates the next cycle. The multiple phosphorylations of PER prior to degradation introduce a time delay, which appears to be important for generating the ~24-h oscillation period. In addition to the negative-feedback loop based on *per* autorepression, positive regulation of *per* and other genes essential for oscillations is also important (Bae *et al.*, 2000). Posttranscriptional regula-

tion of protein synthesis may also be important (Roenneberg and Merrow, 1998). In mammals, several isoforms of PER with distinct functions exist, and the PER proteins in concert with others mediate both negative and positive regulation of core gene transcription (Shearman *et al.*, 2000). As in *Drosophila*, multiple phosphorylations of mammalian PER occur before degradation, and may be important for the 24-h period (Lee *et al.*, 2001).

Models based on differential equations have been developed to represent circadian rhythms and their responses to stimuli. The organism most commonly modeled is *Drosophila* (Goldbeter, 1996; Leloup and Goldbeter, 1998; Smolen *et al.*, 2000). Models for the generation of circadin rhythms in particular species are complex because of multiple genes and biochemical time delays. One recent *Drosophila* model incorporates negative and positive regulation of *per* and other genes, as well as stochastic fluctuations in the numbers of gene product proteins (Smolen *et al.*, 2001). A simpler model, presented here, captures essential processes common to many organisms. To formulate this model, a TF is assumed to repress transcription of its own gene. Newly synthesized TF protein must be multiply phosphorylated prior to degradation. A burst of *tf* transcription is ended by repression due to TF protein accumulation. Then, there is a period of approximately 1 day during which TF protein is phosphorylated and degraded. Degradation allows initiation of another burst of *tf* transcription. A time delay τ is included between transcription of *tf* mRNA and subsequent translation of protein. The model is shown schematically in Fig. 14.14A.

This model simulates circadian oscillations as illustrated in Fig. 14.14B, which displays time courses of mRNA and of total protein concentration. Circadian oscillations are simulated only if multiple (~8 or more) phosphorylations of the TF are assumed necessary prior to degradation. This observation is consistent with experiments in *Drosophila* and other organisms (Dunlap *et al.*, 1999). The necessity for multiple phosphorylations is not surprising. It follows from a general result that increasing the number of kinetic steps in a negative-feedback loop promotes oscillations (Griffith, 1968). Inclusion of the delay τ, with a value of 1–2 h, increases the amplitude and stability of oscillations.

The equations for this model are somewhat complex. P_{0-N} is used to denote a TF with 0, 1, . . ., N phosphorylations, and only P_N is degraded. N takes values of 8–10. k_{ph} is a first-order rate constant governing the rate of every phosphorylation reaction. $[P_{tot}]$ denotes the total concentration of protein, $[P_{tot}] = [P_0] + [P_1] + \ldots + [P_N]$. The differential equation for

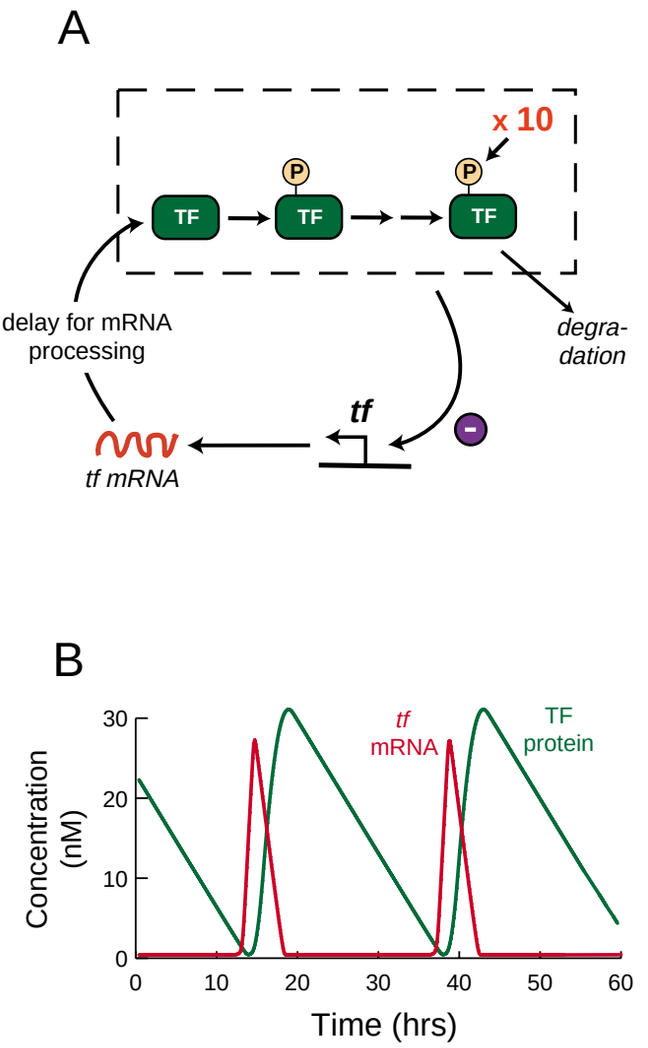

FIGURE 14.14 Generation of circadian rhythmicity by negative transcriptional feedback. (A) The kinetic scheme. A transcription factor (TF) can undergo multiple phosphorylation steps. Ten sequential phosphorylations are assumed. As indicated by the dashed box, all forms of TF protein are assumed capable of repressing *tf* transcription. A time delay is included between the appearance of *tf* mRNA and TF protein. Only fully phosphorylated TF can degrade. But it does so relatively rapidly, so that over the space of a day, virtually all TF protein becomes fully phosphorylated and then degrades. This relieves *tf* repression so that another "burst" of *tf* transcription can occur. (B) Circadian oscillations in the levels of *tf* mRNA and TF protein simulated by the model of (A).

TF mRNA has a synthesis term containing repression by TF protein ($[P_{tot}]$ in the denominator) with a Hill coefficient of n. n is typically 2–4. First-order degradation of mRNA is assumed:

$$\frac{d[\text{mRNA}]}{dt} = v_R \frac{K_R^n}{[P_{\text{tot}}]^n + K_R^n} \pm k_d[\text{mRNA}].$$

Nonphosphorylated TF, P_0, is synthesized from mRNA after a delay τ (typically 1–2 h). P_0 disappears via phosphorylation to P_1:

$$\frac{d[P_0]}{dt} = k_P[\text{mRNA}](t \pm \tau) \pm k_{\text{ph}}[P_0].$$

A series of phosphorylation reactions ensue until the most highly phosphorylated form, P_N, is created. The reactions are assumed sequential so that phosphorylation i cannot occur until phosphorylation i-1 has occurred:

$$\frac{d[P_i]}{dt} = \pm k_{\text{ph}}[P_i] + k_{\text{ph}}[P_{i\pm1}], \quad \text{for } i = 2, \ldots N \pm 1.$$

Finally, P_N is synthesized by phosphorylation and is degraded in a Michaelis–Menten enzymatic reaction:

$$\frac{d[P_{\text{N}}]}{dt} = \pm k_{\text{ph}}[P_{\text{N}\pm1}] \pm \frac{v_{\text{P}}[P_{\text{N}}]}{K_{\text{P}} + [P_{\text{N}}]}.$$

Random Fluctuations in Molecule Numbers Can Strongly Influence Genetic Regulation

As discussed above (Eq. 24 and accompanying text), models using differential equations can be extended to include random variability in the times of individual macromolecular synthesis and degradation events. This variability gives rise to stochastic fluctuations in the numbers of individual mRNAs and proteins. Such fluctuations could strongly influence the dynamics of gene expression. Recent observations indicate that the timing of transcription of individual mRNAs is indeed quite random (Elowitz *et al.*, 2001; Zlokarnik *et al.*, 1998). Also, for important mRNA or protein species the average copy number present in the nucleus may be < 100, so that random fluctuations in copy number may be relatively large. In neurons, late long-term potentiation of synaptic connections lasting 24 h or longer is dependent on transcription and translation. Therefore, stochastic fluctuations in the numbers of mRNAs and proteins may well induce considerable synapse-to-synapse variability in the amount of potentiation.

An example of how fluctuations can destabilize steady states is shown in Fig. 14.15. The simulations for this illustration used a set of four differential equations describing reciprocal regulation of two genes. The regulatory interactions were those of Fig. 14.12. The equations were similar to Eqs. 27a and 28. Figure 14.15A shows that without fluctuations, this model exhibits multistability. Initially, the concentrations of both *tf-1* and *tf-2* mRNA and protein are in a low, stable steady state. As shown, if a temporary increase in the basal transcription rate of *tf-1* is large enough, a transition to a second, stable steady state occurs. Here, the concentrations of *tf-1* mRNA and protein are high, whereas those of *tf-2* mRNA and protein (not shown) are low. In the absence of the transient increase in *tf-1* transcription, the levels of *tf-1* and *tf-2* gene products would not undergo this transition.

Stochastic fluctuations in molecule numbers were then added. The method based on Eq. 24 was used. In this case, when the numbers of each molecular species were initialized at values corresponding to the lower steady state of Fig. 14.15A, this state was no longer stable. After several hours, random fluctuations in molecule numbers would cross a threshold, initiating a positive-feedback loop in which either *tf-1* or *tf-2* would activate its own transcription. Figure 14.15B illustrates that the system would leave the initial state and settle in a new steady state, even without an extrinsic perturbation. In the new state, *tf-1* transcription was high and *tf-2* transcription low. These observations suggest that more generally, stochastic fluctuations can prevent gene networks from settling in states that are only weakly stable.

SUMMARY

Mathematical models are essential for synthesizing large amounts of data concerning intracellular signaling pathway dynamics and regulation of gene expression. Standard modeling techniques have been developed to represent common biochemical elements such as allosteric interactions, feedback interactions in biochemical pathways and gene networks, and intracellular transport of molecules. Modeling of biochemical signaling pathways and of gene networks has suggested a unifying principle—that positive- and negative-feedback interactions commonly underlie complex dynamics of signaling pathways and of gene expression. Such dynamics can include multiple stable states, or oscillations, of biochemical concentrations and reaction rates. Models can also help assess the importance of interactions between signaling pathways.

For extended cells such as neurons, it may be important that models of intracellular signaling include transport of macromolecules or metabolites. Inclusion of random fluctuations in the numbers of particular macromolecules is important if the molecule number per cell is small (several hundred or less). For example, understanding variability in stim-

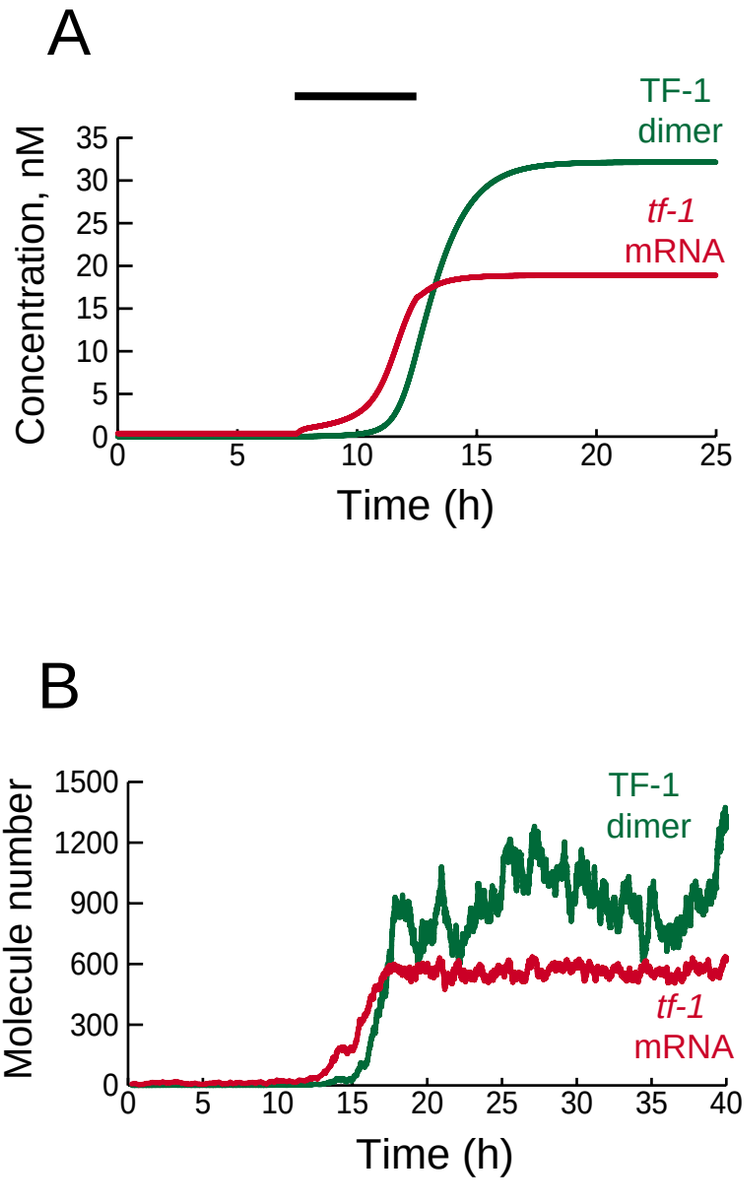

FIGURE 14.15 Stochastic fluctuations in molecule numbers may destabilize steady states of genetic regulatory systems. (A) Without fluctuations, a set of equations based on Fig. 14.12A exhibits multistability. Initial levels of *tf-1* (and *tf-2*) mRNA and protein are low (< 2 nM) and steady. At $t = 7.5$ h the rate of *tf-1* transcription is increased by a constant amount for 10 h (horizontal bar). The increase causes a transition to a stable state with high *tf-1* mRNA and protein levels. The high levels persist after the imposed increase in transcription rate ceases. (B) The initial state of (A) is spontaneously destabilized within ~ 20 h when stochastic fluctuations are incorporated. No induced increase in *tf-1* transcription is included in this simulation, which is otherwise the same as in (A) except for a scaling factor converting the units of the variables from concentrations to molecule numbers.

ulus responses may require consideration of fluctuations in critical mRNAs and proteins. However, sufficient data to constrain models of fluctuations are not available for most signaling pathways or gene networks.

A combination of theory (metabolic control analysis) and experiment has helped determine principles of metabolic flux control in biochemical pathways. For example, the metabolic flux through a pathway is least likely to be sensitive to changes in the activity of enzymes subject to feedback regulation. Use of metabolic control analysis to interpret experimental data can also help determine the rate-limiting reactions for the production of metabolites.

Regulation of gene expression can be modeled at a coarse level, in which genes are ON–OFF switches, or at a finer level, in which gene expression rates are continuous variables. For large gene networks, the coarse method may be the only one feasible, due to limited data. The finer level, using differential equations, is appropriate for networks that can be well characterized experimentally. In gene networks, feedback interactions can generate complex dynamics such as multistability and oscillations. For more realism in models of small gene networks, random fluctuations in macromolecule numbers could be included; however, sufficient data to constrain such models are usually not available.

For all models, it is essential to determine the sensitivity of model behavior to parameters and to assess which parameters are not well constrained by data. Experiments that estimate parameters that are key control points of model behavior constitute stringent tests of a model. Uncertainties in parameters imply that biochemical models are most often qualitative rather than quantitative descriptions of *in vivo* systems. Finally, reduction of the number of model equations to the minimum necessary to simulate experimental data is desirable to help determine the biochemical elements most important for system behavior. Separation of variables according to whether they vary on a fast or slow time scale can help with this simplification.

In conclusion, it is evident that with the biochemical and gene expression data now becoming available, efficient characterization of coupled genetic and biochemical systems will require collaboration between biochemists, molecular biologists, and mathematical biologists. These collaborations will fit data into a mathematical framework and design experiments to test model predictions. This methodology is necessary to predict and analyze the responses of neurons and organisms to physiological stimuli, biologically active environmental contaminants, and novel pharmaceutical agents.

Acknowledgments

We thank Michael Mauk, David Marshak, Neal Waxham, and Jeannie Chin for helpful comments on this chapter.

References

General

Bower, J., and Bolouri, H. (2001). "*Computational Modeling of Genetic and Biochemical Networks*." MIT Press, Cambridge, MA.

Edelstein-Keshet, L. (1988). "*Mathematical Models in Biology*." Random House, New York.

Goldbeter, A. (1996). "*Biochemical Oscillations and Cellular Rhythms*." Cambridge Univ. Press, Cambridge.

Koch, C., and Segev, I. (1998). "*Methods in Neuronal Modeling: From Synapses to Networks*," *2nd ed.* MIT Press, Cambridge, MA.

Murray, J. D. (1989). "*Mathematical Biology*." Springer-Verlag, New York.

Segel, I. H. (1975). "*Enzyme Kinetics*." Wiley, New York.

Smolen, P., Baxter, D. A., and Byrne, J. H. (2000). Mathematical modeling of gene networks. *Neuron* **26**, 567–580.

Specific

Amini, B., Clark, J. W., and Canavier, C. C. (1999). Calcium dynamics underlying pacemaker-like and burst firing oscillations in midbrain dopaminergic neurons, a computational study. *J. Neurophysiol.* **82**, 2249–2261.

Arkin, A., Ross, J., and McAdams, H. (1998). Stochastic kinetic analysis of developmental pathway bifurcation in phage λ-infected *E. coli* cells. *Genetics* **149**, 1633–1648.

Bae, K., Lee, C., Hardin, P. E., and Edery, I. (2000). dCLOCK is present in limiting amounts and likely mediates daily interactions between the dCLOCK-CYC transcription factor and the PER–TIM complex. *J. Neurosci.* **20**, 1746–1753.

Bagley, R. J., and Glass, L. (1996). Counting and classifying attractors in high dimensional dynamical systems. *J. Theor. Biol.* **183**, 269–284.

Barkai, N., and Leibler, S. (2000). Circadian clocks limited by noise. *Nature* **403**, 267–268.

Bartsch, D., Casadio, A., Karl, K., Serodio, P., and Kandel, E. R. (1998). *CREB1* encodes a nuclear activator, a repressor, and a cytoplasmic modulator that form a regulatory unit critical for long-term facilitation. *Cell* **95**, 211–223.

Beck, J. V., and Arnold, K. J. (1977). "*Parameter Estimation n Engineering and Science*," pp. 17–24, 481–487. Wiley, New York.

Berg, O. G., Paulsson, J., and Ehrenberg, M. (2000). Fluctuations and quality of control in biological cells: Zero-order ultrasensitivity reinvestigated. *Biophys. J.* **79**, 1228–1236.

Bhalla, U. S. (2002). Biochemical signaling networks decode temporal patterns of synaptic input. *J. Comp. Neurosci.* **13**, 49–62.

Bhalla, U. S., and Iyengar, R. (1999). Emergent properties of networks of biological signaling pathways. *Science* **283**, 381–386.

Blumenfeld, H., Zablow, L., and Sabatini, B. (1992). Evaluation of cellular mechanisms for modulation of Ca^{2+} transients using a mathematical model of fura-2 Ca^{2+} imaging in *Aplysia* sensory neurons. *Biophys. J.* **63**, 1146–1164.

Brown, G. P., Blitzer, R. D., Connor, J. H., Wong, T., Shenolikar, S., Iyengar, R., and Landau, E. M. (2000). Long-term potentiation induced by θ frequency stimulation is regulated by a protein phosphatase–1-operated gate. *J. Neurosci.* **20**, 7880–7887.

Burden, R. L., and Faires, J. D. (1993). "*Numerical Analysis*." PWS-Kent, Boston.

Busenberg, S., and Mahaffy, J. M. (1985). Interaction of spatial diffusion and delays in models of genetic control by repression. *J. Math. Biol.* **22**, 313–333.

Canavier, C. C., Clark, J. W., and Byrne, J. H. (1993). Simulation of the bursting activity of neuron R15 in *Aplysia*: Role of ionic currents, calcium balance, and modulatory transmitters. *J. Neurophysiol.* **66**, 2107–2124.

Cao, D., and Parker, R. (2001). Computational modeling of eukaryotic mRNA turnover. *RNA* **7**, 1192–1212.

Chen, H. X., Otmakhov, N., Strack, S., Colbran, R. J., and Lisman, J. E. (2001). Is persistent activity of calcium/calmodulin-dependent kinase required for the maintenance of LTP? *J. Neurophysiol.* **85**, 1368–1376.

Cooper, D., Mons, N., and Karpen, J. (1995). Adenylyl cyclases and the interaction between calcium and cAMP signaling. *Nature* **374**, 421–424.

Dano, S., Sorensen, P. G., and Hynne, F. (1999). Sustained oscillations in living cells. *Nature* **402**, 320–322.

Davis, R. J. (2000). Signal transduction by the JNK group of MAP kinases. *Cell* **103**, 239–252.

De Cesare, D., and Sassone-Corsi, P. (2000). Transcriptional regulation by cyclic AMP-responsive factors. *Prog. Nucleic Acid Res. Mol. Biol.* **64**, 343–369.

De Schutter, E., and Smolen, P. (1998). Calcium dynamics in large neuronal models. *In* "*Methods in Neuronal Modeling: From Synapses to Networks*." (C. Koch and I. Segev, Eds.), 2nd ed. MIT Press, Cambridge, MA.

Doedel, E. (1981). AUTO: A program for the automatic bifurcation analysis of autonomous systems. *Congr. Num.* **30**, 265–284.

Dunlap, J. C., Loros, J. J., Liu, Y., and Crosthwaite, S. K. (1999). Eukaryotic circadian systems: Cycles in common. *Genes Cells* **4**, 1–10.

Edwards, A. S., and Scott, J. D. (2000). A-kinase anchoring proteins: Protein kinase A and beyond. *Curr. Opin. Cell Biol.* **12**, 217–221.

Elowitz, M. B., and Leibler, S. (2000). A synthetic oscillatory network of transcriptional regulators. *Nature* **403**, 335–338.

Elowitz, M. B., Levine, A. J., Siggia, E. D., and Swain, P. S. (2001). Stochastic gene expression in a single cell. *Science* **297**, 1183–1186.

Ermentrout, B. (2001). Simplifying and reducing complex models. *In* "*Computational Modeling of Genetic and Biochemical Networks*" (J. Bower and H. Bolouri, Eds.). MIT Press, Cambridge, MA

Ferrell, J. E. (1996). Tripping the switch fantastic: How a protein kinase cascade can convert graded inputs into switch-like outputs. *Trends Biochem. Sci.* **21**, 460–466.

Fink, C. C., Slepchenko, B., Moraru, I., Watras, J., Schaff, J. C., and Loew, L. M. (2000). An image-based model of calcium waves in differentiated neuroblastoma cells. *Biophys. J.* **79**, 163–183.

Firth, C. A., and Bray, D. (2001). Stochastic simulation of cell signaling pathways. *In* "*Computational Modeling of Genetic and Biochemical Networks*." (J. Bower and H. Bolouri, Eds.), MIT Press, Cambridge, MA.

Fokina, K. V., Dainyak, M. B., Nagradova, N. K., and Muronetz, V. I. (1997). A study on the complexes between human erythrocyte enzymes participating in the conversions of 1,3-diphosphoglycerate. *Arch. Biochem. Biophys.* **345**, 185–192.

Frank, P. M. (1978). "*Introduction to System Sensitivity Theory*," pp. 9–10. Academic Press, New York.

Gardner, T. S., Cantor, C. R., and Collins, J. J. (2000). Construction of a genetic toggle switch in *Escherichia coli. Nature* **403**, 339–342.

Gartner, K. (1990). A third component causing variability beside environment and genotype: A reason for the limited success of a 30-year long effort to standardize laboratory animals? *Lab. Anim.* **24**, 71–77.

Gerhold, D., Rushmore, T., and Caskey, C. T. (1999). DNA chips: Promising toys have become powerful tools. *Trends Biochem. Sci.* **24**, 168–173.

Gibson, M. A., and Bruck, J. (2000). Efficient exact stochastic simulation of chemical systems with many species and many channels. *J. Phys. Chem.* A **104**, 1876–1889.

Giese, K. P., Fedorov, N. B., Filipkowski, R. K., and Silva, A. J. (1998). Autophosphorylation at Thr(286) of the alpha calcium-calmodulin kinase II in learning and memory. *Science* **279**, 870–873.

Gillespie, D. T. (1977). Exact stochastic simulation of coupled chemical reactions. *J. Phys. Chem.* **61**, 2340–2361.

Glass, L., and Kauffman, S. A. (1973). The logical analysis of continuous, non linear biochemical control networks. *J. Theor. Biol.* **39**, 103–129.

Goldbeter, A. (1996). "*Biochemical Oscillations and Cellular Rhythms*." Cambridge Univ. Press, Cambridge.

Goldbeter, A., and Koshland, D. E. (1984). Ultrasensitivity in biochemical systems controlled by covalent modification: Interplay between zero-order and multistep effects. *J. Biol. Chem.* **259**, 14441–14447.

Griffith, J. S. (1968). Mathematics of cellular control processes. I. Negative feedback to one gene. *J. Theor. Biol.* **20**, 202–208.

Hanson, P. I., Meyer, T., Stryer, L., and Schulman, H. (1994). Dual role of calmodulin in autophosphorylation of multifunctional CaM kinase may underlie decoding of calcium signals. *Neuron* **12**, 943–956.

Hodgkin, A. L., and Huxley, A. F. (1952). A quantitative description of membrane current and its application to conduction and excitation in nerve. *J. Physiol. (London)* **117**, 500–544.

Holmes, W. R. (2000). Models of calmodulin trapping and CaM kinase II activation in a dendritic spine. *J. Comp. Neurosci.* **8**, 65–85.

Hsich, G., Sena-Esteves, M., and Breakefield, X. O. (2002). Critical issues in gene therapy for neurologic disease. *Hum. Gene Ther.* **13**, 579–604.

Huang, C. F., and Ferrell, J. E. (1996). Ultrasensitivity in the mitogen-activated protein kinase cascade. *Proc. Natl. Acad. Sci. USA* **93**, 10078–10083.

Husi, H., Ward, M. A., Choudhary, J. S., Blackstock, W. P., and Grant, S. G. (2000). Proteomic analysis of NMDA receptor–adhesion protein signaling complexes. *Nat. Neurosci.* **3**, 661–669.

Ihmels, J., Friedlander, G., Bergmann, S., Sarig, O., Ziv, Y., and Barkai, N. (2002). Revealing modular organization in the yeast transcriptional network. *Nat. Genet.* **31**, 370–377.

Jafri, M. S., and Keizer, J. (1995). On the roles of Ca^{2+} diffusion, Ca^{2+} buffers, and the endoplasmic reticulum in IP3-induced Ca^{2+} waves. *Biophys. J.* **69**, 2139–2153.

Karin, M. (1994). Signal transduction from the cell surface to the nucleus through the phosphorylation of transcription factors. *Curr. Opin. Cell Biol.* **6**, 415–424.

Katz, P. S., and Clemens, S. (2001). Biochemical networks in nervous systems: Expanding neuronal information capacity beyond voltage signals. *Trends Neurosci.* **24**, 18–25.

Kaufman, E. N., and Jain, R. K. (1990). Quantification of transport and binding parameters using fluorescence recovery after photobleaching, potential for *in vivo* applications. *Biophys. J.* **58**, 873–885.

Keller, A. (1994). Specifying epigenetic states with autoregulatory transcription factors. *J. Theor. Biol.* **170**, 175–181.

Keller, A. (1995). Model genetic circuits encoding autoregulatory transcription factors. *J. Theor. Biol.* **172**, 169–185.

Kerszberg, M., and Changeux, J. (1998). A simple molecular model of neurulation. *Bioessays* **20**, 758–770.

Kholodenko, B. N., Brown, G. C., and Hoek, J. B. (2000). Diffusion control of protein phosphorylation in signal transduction pathways. *Biochem. J.* **350**, 901–907.

Kurganov, B. I. (1986). The role of multienzyme complexes in integration of intracellular metabolism. *J. Theor. Biol.* **119**, 445–455.

Laurent, M., and Kellershohn, N. (1999). Multistability: A major means of differentiation and evolution in biological systems. *Trends Biochem. Sci.* **24**, 418–422.

Lee, C., Etchegaray, J., Cagampang, F., Loudon, A. S., and Reppert, S. M. (2001). Posttranslational mechanisms regulate the mammalian circadian clock. *Cell* **107**, 855–867.

Leloup, J. C., and Goldbeter, A. (1998). A model for circadian rhythms in *Drosophila* incorporating the formation of a complex between the PER and TIM proteins. *J. Biol. Rhythms* **13**, 70–87.

Levchenko, A., Bruck, J., and Sternberg, P. W. (2000). Scaffold proteins may biphasically affect the levels of mitogen-activated

protein kinase signaling and reduce its threshold properties. *Proc. Natl. Acad. Sci. USA* **97**, 5818–5823.

Li, Y. X., and Rinzel, J. (1994). Equations for $InsP_3$ receptor-mediated $[Ca]_i$ oscillations derived from a detailed kinetic model: a Hodgkin–Huxley-like formalism. *J. Theor. Biol.* **166**, 461–473.

Lisman, J. (1994). The CaM kinase II hypothesis for the storage of synaptic memory. *Trends Neurosci.* **17**, 406–412.

Lisman, J. E., and Zhabotinsky, A. M. (2001). A model of synaptic memory: A CAMKII/PP1 switch that potentiates transmission by organizing an AMPA receptor anchoring assembly. *Neuron* **31**, 191–201.

Little, J. W., Shepley, D. P., and Wert, D. W. (1999). Robustness of a gene regulatory circuit. *EMBO J.* **18**, 4299–4307.

Lonze, B. E., and Ginty, D. D. (2002). Function and regulation of CREB family transcription factors in the nervous system. *Neuron* **35**, 605–623.

MacDonald, N. (1989). "*Biological Delay Systems: Linear Stability Theory*". Cambridge Univ. Press, New York.

Marder, E. (2000). Models identify hidden assumptions. *Nat. Neurosci. Suppl.* **3**, 1198.

Martin, S. J, Grimwood, P. D, and Morris, R. G. (2000). Synaptic plasticity and memory: An evaluation of the hypothesis. *Annu. Rev. Neurosci.* **23**, 649–711.

Mauk, M. D. (2000). The potential effectiveness of simulations verses phenomenological models. *Nat. Neurosci.* **3**, 649–651.

Mayford, M., and Kandel, E. R. (1999). Genetic approaches to memory storage. *Trends Genet.* **15**, 463–470.

McAdams, H., and Arkin, A. (1998). Simulation of prokaryotic genetic circuits. *Annu. Rev. Biophys. Biomol. Struct.* **27**, 199–224.

McAdams, H., and Arkin, A. (1999). It's a noisy business! Genetic regulation at the nanomolar scale. *Trends Genet.* **15**, 65–69.

Mirnics, K., Middleton, F. A., Marquez, A., Lewis, D. A., and Levitt, P. (2000). Molecular characterization of schizophrenia viewed by microarray analysis of gene expression in prefrontal cortex. *Neuron* **28**, 53–67.

Molina, C., Foulkes, N., Lalli, E., and Sassone-Corsi, P. (1993). Inducibility and negative autoregulation of CREM: An alternative promoter directs the expression of ICER, and early response repressor. *Cell* **75**, 875–886.

Morton-Firth, C. J., Shimizu, T. S., and Bray, D. (1999). A free-energy-based stochastic simulation of the Tar receptor complex. *J. Mol. Biol.* **286**, 1059–1074.

Nakamura, T., Barbara, J., Nakamura, K., and Ross, W. N. (1999). Synergistic release of Ca^{2+} from IP_3-sensitive stores evoked by synaptic activation of mGluRs paired with backpropagating action potentials. *Neuron* **24**, 727–737.

Ouyang, Y., Kantor, D., Harris, K. M., Schuman, E. M., and Kennedy, M. B. (1997). Visualization of the distribution of autophosphorylated calcium/calmodulin dependent protein kinase II after tetanic stimulation in the CA1 area of the hippocampus. *J. Neurosci.* **17**, 5416–5427.

Paulsson, J., Berg, O. G, and Ehrenberg, M. (2000). Stochastic focusing: Fluctuation-enhanced sensitivity of intracellular regulation. *Proc. Natl. Acad. Sci. USA* **97**, 7148–7153.

Prentki, M., Tornheim, K., and Corkey, B. E. (1997). Signal transduction mechanisms in nutrient-induced insulin secretion. *Diabetologia* **40** (Suppl. 2), S32–S34.

Press, W. H. (1994). "*Numerical Recipes in C: The Art of Scientific Computing*." Cambridge Univ. Press, Cambridge.

Qian, N., and Sejnowski, T. (1990). When is an inhibitory synapse effective? *Proc. Natl. Acad. Sci. USA* **87**, 8145–8149.

Ramoni, M. F., Sebastiani, P., and Kohane, I. S. (2002). Cluster analysis of gene expression dynamics. *Proc. Natl. Acad. Sci. USA* **99**, 9121–9126.

Reppert, S. M., and Weaver, D. R. (2001). Molecular analysis of mammalian circadian rhythms. *Annu. Rev. Physiol.* **63**, 647–676.

Rinzel, J. (1985). Excitation dynamics: Insights from simplified membrane models. *Fed. Proc.* **44**, 247–264.

Roberts, C. J., Nelson, B., Marton, M. J., Stoughton, R., Meyer, M. R., Bennett, H. A., He, Y. D., Dai, H., Walker, W. L., Hughes, T. R., Tyers, M., Boone, C., and Friend, S. H. (2000). Signaling and circuitry of multiple MAPK pathways revealed by a matrix of global gene expression profiles. *Science* **287**, 873–880.

Roenneberg, T., and Merrow, M. (1998). Molecular circadian oscillators: An alternative hypothesis. *J. Biol. Rhythms* **13**, 167–179.

Rohwer, J. M., Postma, P. W., Kholodenko, B. N., and Westerhoff, H. V. (1998). Implications of macromolecular crowding for signal transduction and metabolite channeling. *Proc. Natl. Acad. Sci. USA* **95**, 10547–10552.

Ryu, D. D., and Nam, D. H. (2000). Recent progress in biomolecular engineering. *Biotechnol. Prog.* **16**, 2–16.

Sabry, J., O'Connor, T., and Kirschner, M. W. (1995). Axonal transport of tubulin in Ti1 Pioneer neurons *in situ*. *Neuron* **14**, 1247–1256.

Salter, M. (1996). Determination of the flux control coefficient of nitric oxide synthase for nitric oxide synthesis in discrete brain regions *in vivo*. *J. Theor. Biol.* **182**, 449–452.

Segel, I. H. (1975). "*Enzyme Kinetics*." Wiley, New York.

Shearman, L. P., Sriram, S., Weaver, D. R., Maywood, E. S., Chaves, I., Zheng, B., Kume, K., Lee, C. C., van der Horst, G., Hastings, M. H., and Reppert, S. M. (2000). Interacting molecular loops in the mammalian circadian clock. *Science* **288**, 1013–1019.

Simon, S., and Llinas, R. (1985). Compartmentalization of the submembrane calcium activity during calcium influx and its significance in transmitter release. *Biophys. J.* **48**, 485–498.

Small, J. R., and Kacser, H. (1993). Responses of metabolic systems to large changes in enzyme activities and effectors. *Eur. J. Biochem.* **213**, 613–640.

Smolen, P., and Keizer, J. (1992). Slow voltage inactivation of Ca^{2+} currents and bursting mechanisms for the mouse pancreatic beta-cell. *J. Membr. Biol.* **127**, 9–19.

Smolen, P., Baxter, D. A., and Byrne, J. H. (1998). Frequency selectivity, multistability, and oscillations emerge from models of genetic regulatory systems. *Am. J. Physiol.* **274**, C531–C542.

Smolen, P., Baxter, D. A., and Byrne, J. H. (1999). Effects of macromolecular transport and stochastic fluctuations on the dynamics of genetic regulatory systems. *Am. J. Physiol.* **277**, C777–C790.

Smolen, P., Baxter, D. A., and Byrne, J. H. (2000). Mathematical modeling of gene networks. *Neuron* **26**, 567–580.

Smolen, P., Baxter, D. A., and Byrne, J. H. (2001). Modeling circadian oscillations with interlocking positive and negative feedback loops. *J. Neurosci.* **21**, 6644–6656.

Stacey, W. C., and Durand, D. M. (2001). Synaptic noise improves detection of subthreshold signals in hippocampal CA1 neurons. *J. Neurophysiol.* **86**, 1104–1112.

Stephanopoulos, G. N., Aristidou, A., and Nielsen, J. (1998). "*Metabolic Engineering, Principles and Methodologies*." Academic Press, San Diego.

Teruel, M. N., and Meyer, T. (2000). Translocation and reversible localization of signaling proteins: A dynamic future for signal transduction. *Cell* **103**, 181–184.

Thomas, R., Thieffry, D., and Kaufman, M. (1995). Dynamical behaviour of biological regulatory networks: I. Biological role of feedback loops and practical use of the concept of the loop-characteristic state. *Bull. Math. Biol.* **57**, 247–276.

Toh, H., and Horimoto, K. (2002). Inference of a genetic network by a combined approach of cluster analysis and graphical Gaussian modeling. *Bioinformatics* **18**, 287–297.

Varga, C. M., Hong, K., and Lauffenburger, D. A. (2001). Quantitative analysis of synthetic gene delivery vector design properties. *Mol. Ther.* **4**, 438–446.

Wagner, A. (2000). Robustness against mutations in genetic networks of yeast. *Nat. Genet.* **24**, 355–361.

Wagner, J., and Keizer, J. (1994). Effects of rapid buffers on Ca^{2+} diffusion and Ca^{2+} oscillations. *Biophys. J.* **67**, 447–456.

Wagner, J., Li, Y. X., Pearson, J., and Keizer, J. (1998). Simulation of the fertilization Ca^{2+} wave in *Xenopus laevis* eggs. *Biophys. J.* **75**, 2088–2097.

Walker, W., Fucci, L., and Habener, J. (1995). Expression of the gene encoding transcription factor CREB: Regulation by follicle-stimulating hormone-induced cAMP signaling in primary rat sertoli cells. *Endocrinology* **136**, 3534–3545.

Wen, X. L., Fuhrman, S., Michaels, G., Carr, D., Smith, S., Barker, J., and Somogyi, R. (1998). Large-scale temporal gene expression mapping of central nervous system development. *Proc. Natl. Acad. Sci. USA* **95**, 334–339.

Wiggins, S. (1990). "*Introduction to Applied Nonlinear Dynamical Systems and Chaos*." Springer-Verlag, Heidelberg.

Yamagata, Y., and Obata, K. (1998). Dynamic regulation of the activated, autophosphorylated state of Ca^{2+}/calmodulin-dependent protein kinase II by acute neuronal excitation *in vivo*. *J. Neurochem.* **71**, 427–439.

Yeung, M. K. S., Tegner, J., and Collins, J. J. (2002). Reverse engineering gene networks using singular value decomposition and robust regression. *Proc. Natl. Acad. Sci. USA* **99**, 6163–6168.

Yin, J., and Tully, T. (1996). CREB and the formation of long-term memory. *Curr. Opin. Neurobiol.* **6**, 264–267.

Zhabotinsky, A. M. (2000). Bistability in the Ca^{2+}/calmodulin-dependent protein kinase–phosphatase system. *Biophys. J.* **79**, 2211–2221.

Zhou, Z., and Neher, E. (1993). Mobile and immobile calcium buffers in bovine adrenal chromaffin cells. *J. Physiol. (London)* **469**, 245–273.

Zimmerman, S., and Minton, A. P. (1993). Macromolecular crowding: biochemical, biophysical, and physiological consequences. *Annu. Rev. Biophys. Biomol. Struct.* **22**, 27–65.

Zlokarnik, G., Negulescu, P., Knapp, T. E., Mere, L., Burres, N., Feng, L., Whitney, M., Roemer, K., and Tsien, R. Y. (1998). Quantitation of transcription and clonal selection of single living cells with β-lactamase as a reporter. *Science* **279**, 84–88.